



1 **Pollen-based climatic reconstructions for the interglacial**
2 **analogues of MIS 1 (MIS 19, 11 and 5) in the Southwestern**
3 **Mediterranean: insights from ODP Site 976**

4
5 Dael Sasso^{1,4}, Nathalie Combourieu-Nebout¹, Odile Peyron², Adele Bertini³, Francesco
6 Toti³, Vincent Lebreton¹, Marie-Hélène Moncel¹

7
8 **corresponding author:*

9 *Dr Dael Sasso (dael.sasso@gmail.com)*

10
11 **Affiliations:**

12 1: UMR 7194, Histoire Naturelle de l'Homme Préhistorique, CNRS-MNHN, Institut de Paléontologie Humaine,
13 Paris, France

14 2: Institut des Sciences de l'Évolution de Montpellier, UMR CNRS 5554 ISEM, Université de Montpellier, France

15 3: Dipartimento di Scienze della Terra, Università di Firenze, Italy

16 4: Geosciences Barcelona (GEO3BCN), CSIC, Lluís Solè i Sabarís s/n, 08028 Barcelona, Spain

17
18 **Abstract**

19 Pleistocene interglacials, specifically MIS 19, 11 and 5, have been suggested as analogues of MIS 1 due to similar
20 solar forcing patterns, greenhouse gas concentrations and sea levels. There has been substantial debate regarding
21 which of these is the most suitable analogue and so far there has been no consensus, although what really emerges
22 from recent work is the high variation in regional climate during these periods. One of the limiting factors in our
23 understanding of these potential analogues is the fact that very few long-sequences cover the entire duration of
24 these interglacials at high resolution.

25 In this study, a multi-method approach is used to produce climatic reconstructions for MIS 19, 11, 5 and 1,
26 using pollen data derived from a single long marine core from ODP Site 976. This represents the first study which
27 attempts to use pollen-based climatic reconstructions to compare MIS 1 with its analogues, representing a
28 necessary contribution to the debate with a focus on the relationships between vegetation and climate in the
29 southwestern Mediterranean.

30 Three methods of quantitative climate reconstruction have been adopted: the more widely used methods
31 Modern Analogues Technique (MAT) and Weighted Average Partial Least Squares regression (WA-PLS), and a
32 more recent machine-learning method known as Boosted Regression Trees (BRT). The reconstructions show
33 consistent changes in temperature and precipitation during MIS 19, 11, 5 and 1, which correlate well with climatic
34 changes observed in other regional and global proxies, and highlight distinct climatic characteristics of each
35 interglacial period in the southwestern Mediterranean. MIS 19 exhibits high variability and colder temperatures
36 compared to subsequent interglacials and the MIS 1. Conversely, MIS 11 displays warmer temperatures and
37 greater stability, which makes it a useful analogue to understand prolonged interglacials, crucial considering the
38 anthropogenic impacts on the duration of warm climate during the Holocene. MIS 5 exhibits overall warmer
39 conditions, and its higher temperature coupled with fluctuations in solar forcing makes it a less suitable MIS 1
40 analogue.

41 Although past interglacials do not offer direct predictions for the Holocene's future, they provide essential
42 insights into Earth's responses to various forcing factors, serving as crucial benchmarks for understanding the
43 Mediterranean's sensitivity to global changes.

44
45 **1. Introduction**

46 The interglacials of the Pleistocene, particularly those of the past 1 Ma (1 million years) and specifically MIS 19
47 (ca. 795–755 ka BP), MIS 11 (ca. 424–365 ka BP) and MIS 5 (ca. 127–78 ka BP), have been source of increasing
48 attention over the past two decades because several of them have been suggested as analogues of the Holocene
49 (e.g. Loutre and Berger, 2003; McManus *et al.*, 2003; Tzedakis, 2010; Candy *et al.*, 2014; Yin and Berger, 2015;
50 Giaccio *et al.*, 2015; Varvus *et al.*, 2018). Studying past interglacials can provide a framework to better evaluate
51 the natural timing and duration of the Holocene, and examining the amplitudes and rates of climatic variability
52 can give an indication of how the current interglacial may have been without anthropogenic interference, and how
53 it could evolve under the presence of humans (Loutre and Berger, 2003; Candy *et al.*, 2014; Giaccio *et al.*, 2015).
54 Furthermore, studying past interglacials may help understand abrupt climate change and the impact of these events
55 on ecosystems and human populations (Loutre and Berger, 2003; Nomade *et al.*, 2019).

56 The selection of the interglacials MIS 19, 11 and 5 is mainly based on their similarities with MIS 1 in terms
57 of astronomical configurations and greenhouse gas (GHG) concentrations (Yin and Berger, 2015). These



58 interglacials are characterised by low eccentricity and similar precession patterns to MIS 1, small variation in
59 insolation amplitudes, and elevated GHGs. However, the search for the best analogue has been source of constant
60 debate (Candy *et al.*, 2014). Chiefly, the arguments have revolved around (1) the best alignment of the insolation
61 patterns between each interglacial and MIS 1, and (2) the structure and duration of these interglacials compared
62 with the Holocene (Candy *et al.*, 2014; Past Interglacials Working Group of PAGES, 2016).

63 MIS 5, specifically substage 5e (ca. 128–116 ka BP)—known as the Eemian (Kukla *et al.*, 1997)—has been
64 previously considered as a modern analogue due to the high temperatures over most of the Northern Hemisphere
65 (NH) and reduced ice sheets (Yin and Berger, 2015). However, the appropriateness of this interglacial was put in
66 question by Loutre and Berger (2003) due to its disproportionately high-amplitude changes in insolation and
67 shorter-lasting high CO₂ concentrations compared to the Holocene.

68 Rather, Loutre and Berger (2003) considered MIS 11 to be closer to MIS 1. Specifically, the climatic optimum
69 of MIS 11c (ca. 427–400 ka BP) has long been recognised as an analogue of the Holocene, owing to similar sea
70 levels, elevated temperatures, reduced astronomical forcing and high atmospheric CO₂ concentrations (McManus
71 *et al.*, 2003; Desprat *et al.*, 2005; Hes *et al.*, 2022). This prolonged and stable period has received further attention
72 because it occurs after one of the harshest glacial conditions of the past 1 Ma (Berger and Loutre, 2003; Raymo
73 and Mitrovica, 2012; Oliveira *et al.*, 2016), which had important implications on the rise of early hominin
74 populations including the spread of Neanderthals and their traditions across Europe and the Mediterranean
75 (Moncel *et al.*, 2016; Blain *et al.*, 2021; Sassoon *et al.*, 2023). The suitability of MIS 11c as an analogue has been
76 supported by several studies (e.g. Berger and Loutre, 2002, 2003; McManus *et al.*, 2003; Olson and Hearty, 2009;
77 Raymo and Mitrovica, 2012). Candy *et al.* (2014) pointed out that this interglacial matches the pattern of solar
78 insolation of the Holocene more closely than any other interglacial of the past 500 ka. However, recent studies
79 have questioned its reliability as analogue due to the unique antiphasing between precession and insolation and
80 obliquity—two precession peaks occurring during one obliquity cycle (Ruddiman, 2007; Tzedakis, 2010; Nomade
81 *et al.* 2019; Tzedakis *et al.*, 2022).

82 Other authors argue that MIS 19 has greater resemblance to the Holocene, owing to a closer phasing of
83 obliquity and precession whereby the maximum obliquity is in phase with the minimum precession at the onset
84 of both interglacials (Tzedakis, 2010). This has been supported by several records in the North Atlantic and
85 Mediterranean (Pol *et al.*, 2010; Tzedakis *et al.*, 2012; Sanchez Goñi *et al.*, 2016; Giaccio *et al.*, 2015; Nomade
86 *et al.*, 2019). This feature, along with similar duration of the climatic optimum, similar mid-June insolation and
87 comparably elevated CO₂ concentrations, has highlighted the viability of MIS 19 as a modern analogue. However,
88 Tzedakis (2010) demonstrated important differences between the trends of GHG concentrations during MIS 19
89 and MIS 1, and the climatic structure of MIS 19. Furthermore, it was found that MIS 19c was generally colder
90 than MIS 5e and MIS 11c (Jouzel *et al.*, 2007), and therefore possibly less climatically comparable to the Holocene
91 especially in the Northern Hemisphere.

92 So far, there has been no consensus on which of these interglacials is the best MIS 1 analogue, and what really
93 emerges from the literature is the high variation in regional climate during MIS 19, 11 and 5. For instance,
94 the appropriateness of MIS 11 as an analogue was supported by McManus *et al.* (2003) in the North Atlantic and
95 by Wang *et al.* (2023) in China, but it was found to be questionable in the Nordic Seas in the study by Bauch *et al.*
96 (2000). This heterogeneity and lack of long cores makes it extremely important to compare these analogues
97 with MIS 1 at a regional scale, using high-resolution records with timeframes that encapsulate the entire
98 interglacials.

99 One region which can help shed some light on this debate is the Mediterranean, due to its high sensitivity to
100 climate change (Lionello and Scarascia, 2018). It is also an area which has been historically affected by
101 anthropogenic pressures, and is likely to be impacted by future warming and drought (Guiot and Cramer, 2016;
102 MedECC 2020; IPCC, 2022), making it imperative to understand the drivers of environmental and climate change
103 across the basin so that we can develop a better framework to predict the trajectory of our current interglacial
104 (Combourieu-Nebout *et al.*, 2015). Moreover, several long cores are available for the Mediterranean region, such
105 as the terrestrial records from Tenaghi Philippon (Pross *et al.*, 2015; Koutsodendrīs *et al.*, 2023), Lake Ohrid
106 (Sadori *et al.*, 2016; Wagner *et al.*, 2019; Donders *et al.*, 2021), Padul (Ortiz *et al.* 2010; Camuera *et al.*, 2018) and
107 marine records from the Iberian Margin (e.g. Sanchez Goñi *et al.*, 2016). Some of these long pollen sequences
108 allowed to quantitatively reconstruct past climate changes during MIS 11 (Kousis *et al.*, 2018), MIS 5 (Sinopoli
109 *et al.*, 2019) and MIS 1 (Peyron *et al.*, 2011, Camuera *et al.* 2021).

110 Recent palynological studies from ODP Site 976 in the Alboran Sea, southwestern Mediterranean, have
111 yielded high-resolution pollen records for MIS 1 (Combourieu-Nebout *et al.*, 2009, 2013; Dormoy *et al.*, 2009),
112 MIS 5 (Masson-Delmotte *et al.*, 2005), MIS 11 (Sassoon *et al.*, 2023) and MIS 19 (Toti *et al.*, 2020), providing a
113 unique opportunity to investigate the regional suitability of these interglacials as analogues of MIS 1 using proxies
114 from a single core. This study aims to provide quantitative estimates of past climate changes for each interglacial
115 by implementing a robust multi-method approach (Peyron *et al.*, 2017; Salonen *et al.*, 2019; Robles *et al.*, 2023),
116 using pollen data derived from the long marine core of ODP Site 976. This approach enables a comparison of



117 Holocene analogues and represents a necessary contribution to the debate on the links between vegetation and
118 climate in the Mediterranean.

119 The objectives of this study are to:

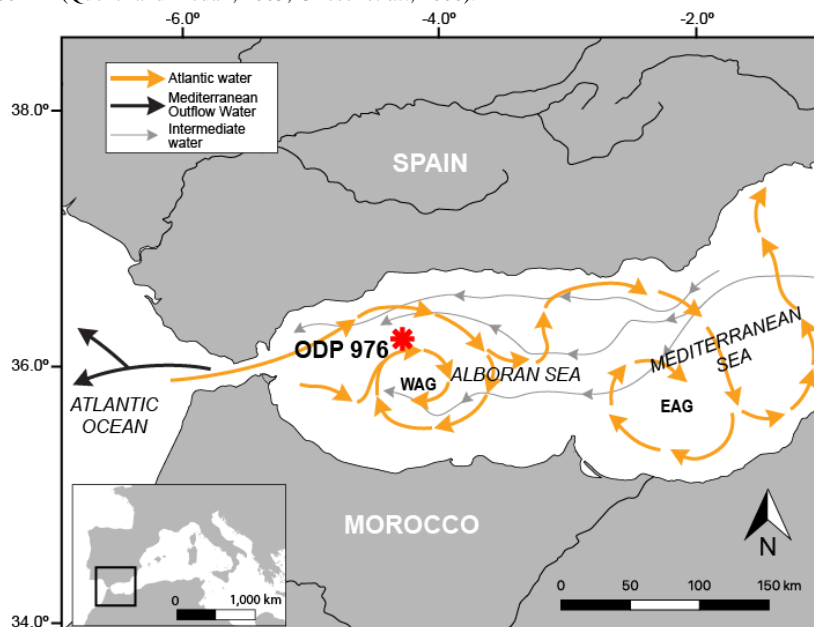
- 120 1. Reconstruct temperature and precipitation parameters during MIS 19, MIS 11, MIS 5 and MIS 1 using
121 a pollen-based multi-method approach
- 122 2. Assess the reliability of multiple quantitative reconstruction methods
- 123 3. Compare climatic variability during the interglacials with local and global proxies
- 124 4. Evaluate the suitability of the interglacials as analogues of the Holocene in the Southwestern
125 Mediterranean.

127 2. Site description

128 This study used pollen records derived from the marine core of the Ocean Drilling Program (ODP) Site 976 in the
129 Western Alboran Sea (36°12.3'N 4°18.8'W), collected in 1999 during leg 161 (Shipboard Scientific Party, 1996).
130 This site (Fig. 1) is located about 110 km off the coast of the Strait of Gibraltar at a depth of 1108 m (Combourieu-
131 Nebout *et al.*, 1999, 2009; Gonzalez-Donoso *et al.*, 2000). Due to its susceptibility to polar, tropical, and Atlantic
132 influences, the Alboran Sea is extremely sensitive to climate changes on centennial and millennial scales, making
133 it an ideal location to study climatic variability and interglacial comparisons Alonso *et al.*, 1999; Combourieu-
134 Nebout *et al.*, 1999, 2002, 2009; Fletcher and Sanchez Goñi, 2008; Dormoy *et al.*, 2009; Toti *et al.*, 2020; Bulian
135 *et al.*, 2022).

136 The Alboran Sea measures 150 km in width and 350 km in length, forming a narrow extensional basin (Alonso
137 *et al.*, 1999) between the Mediterranean Sea to the east and the Atlantic Ocean to the west (Bulian *et al.*, 2022).
138 The northern coast of the basin borders with Spain while it borders with Morocco to the south. The Alboran Sea
139 is dominated by water circulation which is predominantly a result of the exchange of waters at the Strait of
140 Gibraltar whereby low-salinity waters from the Atlantic enter the basin and high-salinity waters from the
141 Mediterranean outflow into the ocean (Bulian *et al.*, 2022). This results in the Eastern Alboran Gyres (EAG) and
142 the Western Alboran Gyres (WAG) (Bulian *et al.*, 2022), two anti-cyclonic gyres (fig. 1).

143 This part of the Mediterranean is affected by the Southern Azores cyclone resulting in long, dry summers with
144 mean temperatures typically exceeding 20°C. In contrast, winters are mild and rainy, with temperatures ranging
145 10°C on the coast and -7°C at higher elevations resulting in an altitudinal gradient; annual precipitation is usually
146 400–1400 mm (Quézel and Médail, 2003; Grieser *et al.*, 2006).



147

148 **Figure 1 - Map showing the location of ODP Site 976 and the present-day surface and water circulation in**
149 **the Alboran Sea (modified from Combourieu-Nebout *et al.*, 1999).**

150



151 Vegetation cover is a function of an altitudinal gradient owing to the presence of the Moroccan Rif and Betic
152 Cordillera (Quézel and Medail, 2003). The coast is dominated mainly by steppe with *Lygeum*, *Artemisia* and
153 Mediterranean taxa (e.g. *Olea*, *Phillyrea*, *Pistacia*, and *Quercus ilex*). Humid-temperate oak forest with *Quercus*
154 *deciduous* and Ericaceae dominates the mid-altitudes. Higher elevations are mainly characterised by cold-
155 temperate coniferous forests with *Pinus* and *Abies*. Although once more spread in the Mediterranean, *Cedrus* is
156 only found now at higher elevations in Morocco (Ozenda, 1975; Rivas Martinez, 1982; Barbero *et al.*, 1981;
157 Benabid, 1982).

158

159 **3. Methods**

160

161 3.1 Fossil pollen datasets

162 The fossil pollen datasets used to run the pollen-based quantitative climatic reconstructions are all obtained from
163 the ODP Site 976 marine record from the studies listed below. All records excluded *Pinus*, due to its
164 overrepresentation in marine samples (Heusser and Balsam, 1977; Naughton *et al.*, 2007). The ages used in this
165 study are in calendar ka (cal ka).

- 166 - The pollen record for MIS 19 (Toti *et al.*, 2020) comprises 102 samples. The chronology was based on the
167 initial age models from de Kaenel *et al.* (1999) and Grafenstein *et al.* (1999). Samples were taken every
168 10 cm, yielding an average temporal resolution of 450 years between samples.
- 169 - The pollen record for MIS 11 has a total of 141 samples (Sassoon *et al.*, 2023). The chronology for the
170 fossil pollen record is based on von Grafenstein *et al.* (1999). Age interpolation revealed a lowermost age
171 of 433.868 ka BP at 118.8 m and an uppermost age of 356.456 ka BP at 98.85 m. The pollen record for
172 MIS 11 has an almost consistent resolution of 10 cm, achieving average temporal resolutions of ca. 128
173 years between samples.
- 174 - The MIS 5 record has 105 samples (Combourieu-Nebout *et al.*, 2002; Masson-Delmotte *et al.*, 2005). The
175 chronology for this record was based on the age model by Combourieu-Nebout *et al.* (2002) but has been
176 extended to 130 ka BP by correlation with deep sea core MD95-2042 (Shackleton *et al.*, 2003) and
177 NorthGRIP $\delta^{18}\text{O}$ record (NorthGRIP, 2004). Samples were taken at an average resolution of 10 cm,
178 yielding an average temporal resolution of 500 years between samples.
- 179 - The record for MIS 1 was based on the uppermost 10m of the ODP Site 976 core, with a total of 136
180 samples (Combourieu-Nebout *et al.*, 2009). The chronology is built on ten ^{14}C AMS radiocarbon ages,
181 specifically measured on monospecific samples of *Globigerina bulloides* and *Neogloboquadrina*
182 *pachyderma*, which revealed a lowermost age of 25 cal ka. The pollen analysis involved sampling at 10
183 cm intervals, with a higher resolution of 1–5 cm for the Bølling/Allerød and the early Holocene, yielding
184 a resolution which varies from ~20–40 years during the abrupt events to 200–500 years elsewhere.

185

186 3.2 Pollen-based climate reconstructions methods

187 Three methods of climate reconstruction have been used to derive quantitatively changes in temperature and
188 precipitation parameters for the ODP Site 976 pollen records: Modern Analogues Technique (MAT; Guiot, 1990),
189 Weighted Average Partial Least Squares regression (WA-PLS; Ter Braak and Juggins, 1993) and Boosted
190 Regression Trees (BRT; Salonen *et al.*, 2014).

191 MAT and WA-PLS have been previously used for climate reconstruction focusing on different time periods
192 in the Mediterranean region on both terrestrial and marine pollen records (e.g. Cheddadi *et al.*, 1998; Davis *et al.*,
193 2003; Pross *et al.*, 2009; Peyron *et al.*, 2011, 2013, 2017; Joannin *et al.*, 2012; Kotthoff *et al.*, 2008; Dormoy *et al.*,
194 2009; Sanchez Goñi *et al.*, 2012; Desprat *et al.*, 2013; Sadori *et al.*, 2013; Mauri *et al.*, 2015; Kousis *et al.*,
195 2018; Ardenghi *et al.*, 2019; Sinopoli *et al.*, 2019; Koutsodendris *et al.*, 2019; Robles *et al.*, 2023; Herzschuh *et al.*,
196 2023). The results are often well-supported by other Mediterranean records and independent proxies such as
197 alkenones and other biomarkers, $\delta^{18}\text{O}$ isotopes and sea surface temperature reconstructions, showing the reliability
198 of these methods.

199 MAT uses the present-day environment to quantitatively reconstruct past climate derived from fossil
200 assemblages (Chevalier *et al.*, 2020). MAT functions by determining the degree of dissimilarity between past
201 pollen assemblages and modern pollen data. By using squared-chord distance calculations, MAT selects a number
202 of modern pollen data considered as analogues for each fossil pollen assemblage to infer past climatic values
203 (Guiot, 1990).

204 In contrast to the MAT which is an “assemblages approach”, the WA-PLS method is a true transfer function
205 meaning that it requires statistical calibration between the climate parameters and modern pollen assemblages
206 (Chevalier *et al.*, 2020). It is a regression method which supposes the unimodal relationship between pollen
207 percentages and climate parameters.

208 In comparison to the other methods, BRT is a machine learning method developed for ecology (De'ath, 2007;
209 Elith *et al.*, 2008) and has recently been adopted for palaeoecology and palaeoclimatic reconstructions (Salonen
210 *et al.*, 2014). It uses random binary splitting and cross-validation to predict the relationship between climatic



211 variables and pollen assemblages (Chevalier *et al.*, 2020). In BRTs, great numbers of simple regression-tree
212 models are combined to produce a final model optimised for prediction, using cross-validation for model building.
213 This approach is promising for Mediterranean terrestrial records (Robles *et al.*, 2023; d'Oliveira *et al.*, 2023) but
214 has never been tested on marine pollen records or indeed records of the Mid-Pleistocene.

215 All three methods were calibrated using an updated version of the high-quality and taxonomically consistent
216 modern pollen dataset (Peyron *et al.*, 2013; Dugerdil *et al.*, 2021) containing 3,267 samples from European and
217 Mediterranean regions. *Pinus* has been omitted because its overrepresentation in the Mediterranean pollen
218 spectrum could mask climatically-related signals from other taxa (Sinopoli *et al.*, 2019).

219 In this study, we reconstructed the following climatic parameters: (1) mean annual temperature (TANN); (2)
220 mean temperatures of the coldest month (Twin) and (3) warmest month (Tsum); (4) mean annual precipitation
221 (PANN); (5) summer precipitation (Psum); (6) winter precipitation (Pwin). The entire dataset includes the
222 parameters for growing degree days above 5°C (GDD5), the ratio of actual over potential evapotranspiration
223 (AET/PET), and further seasonal parameters including autumn and spring temperature and precipitation (Taut and
224 Tspr, Paut and Pspr, respectively). The studies by Combourieu-Nebout *et al.* (2009) and Dormoy *et al.* (2009),
225 which implement pollen-based reconstructions for MIS 1 using pollen data from ODP Site 976, represent a crucial
226 foundation for the present paper. While providing guidance, however, these previous studies only applied the
227 MAT method, therefore the application of new methods is necessary to enable the comparison with the results for
228 the other Holocene analogues.

229 Quantitative reconstruction methods and reliability tests were carried out with the software R using the
230 package 'rioja' (Juggins, 2020). The reliability of pollen-inferred climate reconstruction methods was estimated
231 through bootstrapping cross-validation by calculating the correlation coefficient values between the variables (R^2),
232 and using the Root Mean Square Error (RMSE) criterion. Higher R^2 and lower RMSE indicate greater validity of
233 the reconstructed parameters. Loess smoothing of 0.2 was applied to the raw data in the plots to view the overall
234 trends of the parameters.

235

236 **4. Results and discussion**

237

238 **4.1 Multi-method approach: reliability and differences between the methods**

239 The temperature and precipitation reconstructions for the three methods yielded coherent results for the
240 interglacials and interstadials investigated, aligning reasonably with trends observed in other regional climatic
241 proxies (section 4.2).

242 A comparison of the methods across the four interglacials, based on the R^2 and RMSE values, reveals
243 discrepancies in the performance trends. To exemplify these differences between methods, the R^2 and RMSE
244 results for TANN and PANN are shown in table 1. Overall, the models reconstruct TANN more consistently than
245 PANN, based on the significant difference between the RMSE values for these parameters across all MIS periods.
246 BRT consistently demonstrates robust performance, with high R^2 values ranging from 0.918 to 0.920 for TANN
247 and 0.822 to 0.826 for PANN, alongside low RMSE values compared to the other methods. The MAT method,
248 akin to BRT, shows strong performance with high R^2 values ranging from 0.865 to 0.866 for TANN and slightly
249 lower values of 0.711 to 0.713 for PANN, alongside comparatively low RMSE values. However, in comparison
250 to BRT, the MAT method tends to have slightly lower R^2 and higher RMSE, and there is a greater degree of
251 fluctuation for the parameters reconstructed which is interpreted as greater sensitivity to changes in the pollen
252 assemblages. In contrast, WA-PLS exhibits lower R^2 values (ranging from 0.445 to 0.683) and higher RMSE
253 values (ranging from 4.271 to 232.650) across both TANN and PANN parameters, indicating potentially poorer
254 model performance compared to BRT and MAT. Notably, BRT and MAT methods demonstrate greater
255 consistency in performance across interglacials and parameters compared to WA-PLS, suggesting their superior
256 efficacy in reconstructing climatic parameters across different temporal periods.

257 The observed trends in performance of the methods for TANN and PANN are applicable across all parameters
258 reconstructed (see supplementary data); BRT and MAT consistently exhibit strong performance characterized by
259 high R^2 values and low RMSE scores for all reconstructed parameter, while the WA-PLS method has lower R^2
260 values and higher RMSE scores across the board, suggesting a tendency toward less accurate reconstructions.

261

262

263

264

265

266

267

268

269



Table 1 – R² and RMSE results from the methods BRT, WA-PLS and MAT for selected parameters (TANN and PANN) for the interglacials analysed in this study.

		MIS 1		MIS 5		MIS 11		MIS 19	
		R ²	RMSE	R ²	RMSE	R ²	RMSE	R ²	RMSE
BRT	TANN	0.918	2.965	0.919	2.960	0.920	2.962	0.919	2.947
	PANN	0.826	175.89 2	0.822	176.922	0.825	176.590	0.823	176.822
WA-PLS	TANN	0.683	4.271	0.683	4.275	0.683	4.277	0.683	4.275
	PANN	0.453	232.51 8	0.453	232.646	0.453	232.552	0.445	232.650
MAT	TANN	0.865	3.067	0.866	3.063	0.865	3.072	0.865	3.067
	PANN	0.713	184.26 1	0.712	184.385	0.711	187.333	0.711	183.010

270

271

272

273

274

275

276

277

278

279

280

281

282

283

284

285

286

287

288

289

290

291

292

293

294

295

296

297

298

299

300

301

302

303

304

305

306

307

308

309

310

311

312

313

4.2 Climatic reconstructions for each interglacial

4.2.1 MIS 20–19 (803–748 ka BP)

The reconstructions for MIS 20–19 show large-amplitude changes in temperature and precipitation (Fig. 2, Tab. 2). During the period reconstructed for the MIS 20 glacial between 803–786 ka BP, results indicate a cold and dry climate, linked to the occurrence of steppic and semi-desertic taxa such as *Artemisia*, *Amaranthaceae* and *Ephedra*, which are adapted to cold climates (Toti *et al.*, 2020). Throughout MIS 20, TANN fluctuates around 4.7 °C, with PANN averaging approximately 460 mm/yr, although there is a contrast between the periods 803–800 ka BP and 799–787 ka BP (Fig. 2, Tab. 2). In the former period, PANN is around 600 mm/yr and Pwin around 200 mm/yr, while in the latter period PANN decreases to below 400 mm/yr and Pwin to below 50mm/yr (Fig. S2). The transition to harsher conditions during the late MIS 20 (around 799 ka BP) was associated with colder conditions, as evidenced by palynological and foraminiferal records (Toti *et al.*, 2020). This corresponds to a shutdown of the Atlantic Meridional Overturning Circulation (AMOC) during that time (Cacho *et al.*, 2000; Moreno *et al.*, 2004). Maiorano *et al.* (2016) observed this in the Montalbano Jonico section (southern Italy) and referred to it as a Heinrich-type event (Med-HTIX) in analogy to those of the last termination (TI), and similarly the warm-cold episodes during TIX have been named the Bølling-Allerød-like (Med-BATIX) and Younger-Dryas-like (Med-YDTIX) events (Maiorano *et al.*, 2016).

From 788–774 ka BP, the reconstructions for TANN indicate a rise from 2–7 °C during the glacial to 6–13 °C, indicating the transition to MIS 19 (Fig. 2). This period is equivalent to the climatic optimum MIS 19c. This trend is also indicated by PANN, which increases from 350–500 mm during the glacial to between 600–800 mm across the three methods during the climatic optimum, indicating warmer and wetter conditions compared to MIS 20 (Toti *et al.*, 2020). This climatic amelioration is interrupted by a short-lived event to cooler and drier conditions and a change in seasonality around 785 ka BP. This event has been observed in other pollen records including Montalbano Jonico (Bertini *et al.*, 2015) and speleothem records like Sulmona (Regattieri *et al.*, 2019).

In the Alboran Sea, a peak in warmth and humidity is observed around 778 ka BP throughout the three methods, although some differences in the methods are observed, where WA-PLS and BRT suggest a more gradual temperature and precipitation increase than MAT, which indicates greater amplitude fluctuations (Fig. 2). TANN averages between 5 and 10°C and PANN is around 500–700 mm/yr, with Pwin values of around 150–300 mm/yr and Twin around 0°C, suggesting temperate summers and mild winters during MIS 19c (Fig. 2, Fig. S2). These reconstructions correlate well (Fig. 2) with the progressive increase in CH₄ and CO₂ observed in the EPICA ice cores (Jouzel *et al.*, 2007; Nehrbass-Ahles *et al.*, 2020), and decline in Atlantic δ¹⁸O (e.g. Voelker *et al.*, 2010; Oliveira *et al.*, 2016).

There is a decisive fall in temperature centred between 774–771 ka BP, along with a slight decrease in precipitation (Tab. 2), consistent with a return to colder and drier conditions during MIS 19b-a (Toti *et al.*, 2020). T_{win} fluctuates from -9°C to 7°C, indicating substantial variability in winter temperatures, while T_{sum} ranges from 13°C to 22°C, suggesting fluctuations in summer warmth (Fig. S2). TANN varies between 0°C and 14°C, indicating overall climatic changes throughout the year. PANN ranges from 370 mm to 750 mm, reflecting fluctuations in annual precipitation levels. This is followed by three large-amplitude fluctuations during MIS 19a (Fig. 2, Tab. 2), with extreme peaks at 770 and 765 ka BP, separated by two significant events of climatic deterioration at 768 and 764 ka BP, which are linked to the high frequency alternation between forested and open vegetation observed in the pollen record. This shows good agreement with oscillations in the benthic δ¹⁸O record of Montalbano Jonico from Nomade *et al.* (2019), who labelled these 19a-1, 19a-2 and 19a-3. These fluctuations also correlate well with those observed in the benthic δ¹⁸O record from Sulmona (Giaccio *et al.*, 2015; Regattieri



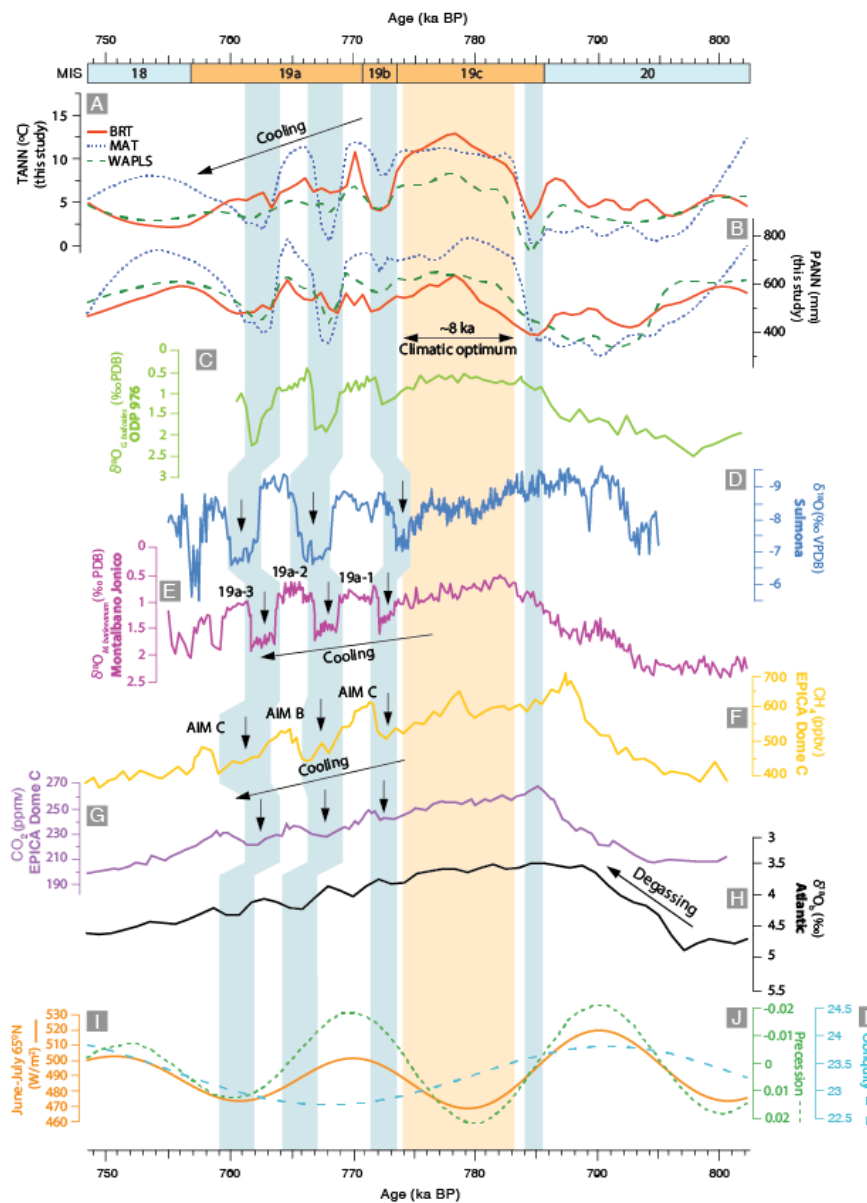
314 *et al.*, 2019), Atlantic $\delta^{18}\text{O}$ (e.g. Voelker *et al.*, 2010; Oliveira *et al.*, 2016) as well as the CH_4 (Loulergue *et al.*,
315 2008) and CO_2 observed in the EPICA ice cores (Jouzel *et al.*, 2007; Nehrass-Ahles *et al.*, 2020). These climatic
316 oscillations may have been caused by a shift in the position of the ITCZ causing northward pressure on the
317 Mediterranean leading to more arid summers and enhanced winter precipitation (Toti *et al.*, 2020).
318

Table 2 – Summary of results of the pollen-based climatic reconstructions for MIS 20–19

Interval	Age (ka BP)	Summary
MIS 19a and 19b	773–756	Decisive fall in temperature centred between 773–771 ka BP. Slight decrease in precipitation but to a lesser extent and consistent with a return to colder and drier conditions. Three large-amplitude fluctuations with extreme peaks at 770 and 765 ka BP, separated by two significant events of climatic deterioration at 768 and 764 ka BP. Continued large-amplitude changes in temperature and precipitation.
MIS 19c climatic optimum	786–773	TANN shows a rise from 2–7 °C during the glacial to 6–13 °C. PANN increases from a range of 350–500 mm during the glacial to between 600–800 mm. MAT suggests the largest changes in both temperature and precipitation. Peak in warmth and humidity observed synchronously around 778 ka BP.
MIS 20/19 transition	803–786	MAT suggests the largest changes in both temperature and precipitation during this transition. Shift from glacial conditions (MIS 20) to interglacial conditions (MIS 19).



319



320
 321 **Figure 2 – Comparison of the pollen-based quantitative reconstructions from ODP976 for MIS 19, (A)**
 322 **TANN and (B) PANN (BRT=red solid line; MAT=blue dotted line; WA-PLS=green dashed line), with other**
 323 **regional and global proxies: (C) $\delta^{18}O_{G. bulloides}$ record from ODP976 (Toti et al., 2020); (D) $\delta^{18}O$ records of**
 324 **Sulmona basin sediments (Regattieri et al., 2019); (E) $\delta^{18}O_{M. barleeanum}$ record from Montalbano Jonico**
 325 **(Nomade et al., 2019); (F) Methane (CH_4) atmospheric concentrations (Louergue et al., 2008) and (G) CO_2**
 326 **atmospheric concentrations from Antarctic EPICA Dome C ice cores (Nehrbass-Ahles et al., 2020); (H)**
 327 **Atlantic $\delta^{18}O$ (Voelker et al., 2010); (I) Summer insolation (Laskar et al., 2004); (J) Precession index and**
 328 **(K) Obliquity curve (Berger and Loutre, 1991). Orange band indicates the period encompassing the**
 329 **climatic optimum, and the blue bands highlight major millennial-scale climatic events.**



330

331 4.2.2 MIS 12–11 (434–356 ka BP)

332 Between 434 and 427 ka BP, reconstructions for the end of MIS 12 show a generally cold and dry climate (Fig.
333 3). Annual temperature reconstructions reveal consistently low values across methods, with the coldest period
334 occurring before 430 ka BP (Tab. 3). During this period, Twin shows temperatures ranging $-5-0^{\circ}\text{C}$ and Tsum
335 does not rise above 17°C (Fig. S3). Following a brief warming around 430 ka BP, a rapid return to colder
336 conditions is observed at 428–426 ka BP across all three methods (Fig. 3). This abrupt shift to colder conditions
337 coincides with decreased sea surface temperatures (SSTs) and increased $\delta^{18}\text{O}_{G. bulloides}$ in the record from the same
338 ODP976 core by Brice (2007), who made the analogy with a Younger Dryas-like (YD-1) event. Other studies refer
339 to this as the Ht4 Heinrich-type event (Hodell *et al.*, 2008; Rodrigues *et al.*, 2011; Girone *et al.*, 2013; Marino *et*
340 *al.*, 2018). Vázquez Riveiros *et al.* (2013) noted enhanced Ice Rafted Debris (IRD) coeval with a sudden decrease
341 in North Atlantic SSTs during this event, indicating significant ice-rafting. Other pollen-based reconstructions,
342 particularly those from Lake Ohrid which used the MAT method (Kousis *et al.*, 2018), show a short-lived decrease
343 in temperatures, precipitation, and forest cover prior to the onset of warmer and wetter conditions during
344 Termination V.

345 From 427 to 405 ka BP, a period with consistently high temperatures and precipitation are observed (Fig. 3,
346 Tab. 3), consistent with the warmest part of MIS 11, substage MIS 11c (Sassoon *et al.*, 2023). This transition has
347 also been observed in other records (Fig. 3) in the Mediterranean region (Tzedakis, 2010; Girone *et al.*, 2013;
348 Kousis *et al.*, 2018; Koutsodendris *et al.*, 2019; Ardenghi *et al.*, 2019; Azibeiro *et al.*, 2021), the North Atlantic
349 off the Iberian coast (Desprat *et al.*, 2005; Oliveira *et al.*, 2016) and continental Europe (Reille and de Beaulieu,
350 1995). TANN rises from around 8°C to $\sim 10-15^{\circ}\text{C}$, over the timeframe of ca. 2,000 years. BRT and WA-PLS
351 show Tsum values of around 18°C , while the MAT method estimates warmest-month temperatures of over 22°C
352 (Fig. S3). This warming is in agreement with the expansion of forest biomass observed in several other records
353 from across the Mediterranean basin throughout Termination V including Lake Ohrid (Kousis *et al.*, 2018),
354 Tenaghi Philippon (Wijmstra and Smit, 1976; Tzedakis *et al.*, 2006; Pross *et al.* 2015; Ardenghi *et al.*, 2019;
355 Koutsodendris *et al.*, 2023) and Bouchet/Praclaux (Reille and de Beaulieu, 1995). This increase in temperatures
356 during MIS 11c may be linked to the MIS 11.3 light isotopic event (Oliveira *et al.*, 2016) and the highest summer
357 insolation recorded for MIS11 in the Northern Hemisphere (Sassoon *et al.*, 2023). The warming trend is also
358 coeval with the rise in Antarctic air temperatures and Atlantic CO_2 records (Fig. 3) (Jouzel *et al.*, 2007; Loulergue
359 *et al.*, 2008; Nehrbass-Ahles *et al.*, 2020). These results correlate with the highest SSTs, highest CO_2 and CH_4
360 concentrations (Jouzel *et al.*, 2007; Nehrbass-Ahles *et al.*, 2020), and reduced $\delta^{18}\text{O}$ (e.g. Voelker *et al.*, 2010;
361 Oliveira *et al.*, 2016).

362 Precipitation also increases during the climatic optimum, suggesting warm and humid conditions (Fig. 3, Tab.
363 3). Annual precipitation results from BRT and WA-PLS show a rise from 500 mm/yr during the glacial to 600
364 mm/yr for MIS 11c in the period between 429–427 ka BP, while MAT suggests a larger amplitude of change from
365 around 380 mm/yr to 600 mm/yr. These results are consistent with pollen-based quantitative reconstructions of
366 Kousis *et al.* (2018) at Lake Ohrid, which suggest a shift to more a humid and warmer climate at the beginning of
367 MIS 11c. However, the reconstructions for precipitation at Lake Ohrid are comparatively higher than the results
368 for ODP 976, evidenced by a rise in PANN to 800–1000 mm/yr at Lake Ohrid (Kousis *et al.*, 2018). At Tenaghi
369 Philippon, precipitation reconstructions derived from calcium/iron ($\log(\text{Ca}/\text{Fe})$) ratio by Koutsodendris *et al*
370 (2023) show that MIS 11c was one of the wettest interglacials at this site with a significant difference between the
371 climatic optimum and the rest of MIS 11. This is a significant finding because this corroborates the hypothesis
372 put forward by several authors (Kandiano *et al.*, 2012; Kousis *et al.*, 2018; Sassoon *et al.*, 2023) who suggested,
373 on the basis of pollen assemblages, that during MIS 11c, the climate in the southwestern Mediterranean was
374 warmer and drier than Lake Ohrid and Tenaghi Philippon in the Balkan Peninsula. Although this might be an
375 effect of a difference in altitude between the sites (which might also explain the difference in annual temperature)
376 and the nature of the substrates observed (marine vs. terrestrial), it might be indicative of an easterly humidity
377 gradient within the wider region owed to the formation of a bipolar see-saw pattern in precipitation between the
378 western and eastern Mediterranean possibly caused by a weakening of the AMOC during the deglaciation (Kousis
379 *et al.*, 2018).

380 During the MIS 11c optimum, a noteworthy fluctuation occurs around 408 ka BP, mainly indicated in our
381 reconstructions by a decrease in PANN (Fig. 3). This is related to a moderate-intensity contraction in temperate
382 and Mediterranean forests (Sassoon *et al.*, 2023). Oliveira *et al.* (2016) and Kousis *et al.* (2018) have linked this
383 forest contraction with the “Older Holstenian Oscillation” (OHO), also found in other records from Europe (West,
384 1956; Kelly, 1964; Turner, 1970; Kukla, 2003; Koutsodendris *et al.*, 2011, 2012, 2023; Tye *et al.*, 2016). Our
385 reconstructions indicate a reduction in TANN by about $1-2^{\circ}\text{C}$, and in PANN by 50 mm/yr on average across the
386 three methods. This appears to be less intense than the changes inferred for Lake Ohrid (Kousis *et al.*, 2018) or
387 Tenaghi Philippon (Ardenghi *et al.*, 2019), which suggest a higher amplitude of change in both precipitation and
388 temperature in the Balkans.



389 Between 400 and 356 ka BP, the substages MIS 11a and 11b exhibit reduced climate variability. Around
 390 400–390 ka BP, a synchronous decline across the reconstructions for temperature and precipitation is interpreted
 391 as a cooler and drier phase, recognized as MIS 11b, connected to a decrease in summer insolation. The
 392 reconstructions show a decline in temperature and precipitation parameters centred around 398 ka BP (Fig. 3).
 393 Similarly, reconstructions for Lake Ohrid demonstrate reductions in TANN and PANN (Kousis *et al.*, 2018),
 394 indicating a synchronous cooling on land and the sea. Around 390–367 ka BP, recognised as substage MIS 11a,
 395 a return to warmer and more humid conditions, though relatively less temperate as he conditions during MIS 11c,
 396 are observed. Temperature reconstructions vary depending on methods, with WA-PLS and BRT indicating less
 397 variation than MAT suggests. PANN and Pwin also increase compared to previous levels at the end of MIS 11b,
 398 showing high variability during MIS 11a (Fig. 3, Fig. S3). Overall, however, these trends correlate with patterns
 399 observed in palaeoclimatic records from the North Atlantic and Mediterranean and seem to reflect summer
 400 insolation (Candy *et al.*, 2014, 2024).

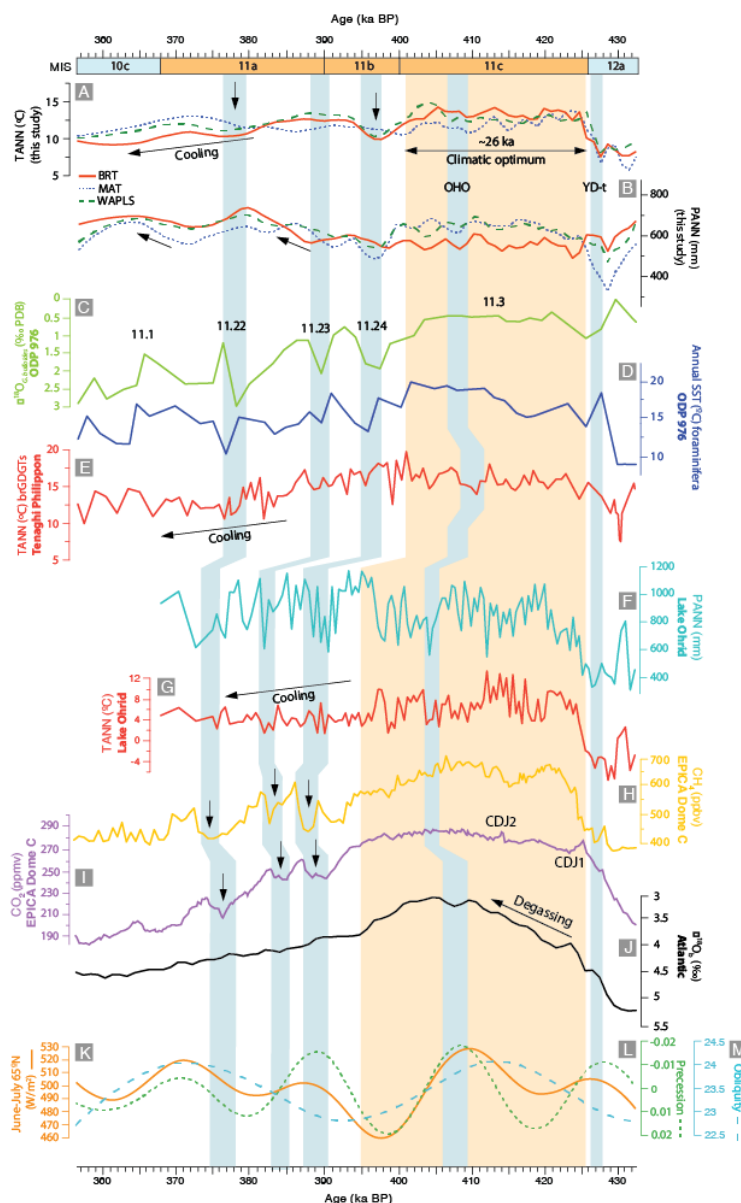
401 The fluctuations during MIS 11a and 11b can be correlated with the light isotopic events 11.24, 11.23 and
 402 11.22 (Fig.3), observed in $\delta^{18}\text{O}$ records (Brice, 2007; Desprat *et al.*, 2005; Oliveira *et al.*, 2016). Particularly, the
 403 drop in precipitation and temperature around 397 ka BP, reflective of the rise in steppe taxa in ODP 976, is
 404 synchronous with light isotopic event 11.24, also observed at IODP Site U1385 (Oliveira *et al.*, 2016), MD01-
 405 2447 (Desprat *et al.*, 2005, 2007), at Lake Ohrid (Kousis *et al.*, 2018), and at Tenaghi Philippon (Ardenghi *et al.*,
 406 2019). The alkenone-based SST record from MD03-2699 show reductions to $\sim 10^\circ\text{C}$ (Rodrigues *et al.*, 2011). This
 407 trend can also be compared with falls in CO_2 and CH_4 concentrations in the Antarctic EPICA records, which
 408 exemplify the sensitivity of the Mediterranean to global-scale climate change.

409 From 367 ka BP onwards, the temperature and precipitation reconstructions across all methods collectively
 410 suggest a transition to a significantly colder and drier climate, consistent with the beginning of the glacial inception
 411 of MIS 10.
 412

Table 3 - Summary of results of the pollen-based climatic reconstructions for MIS 12–11

Interval	Age (ka BP)	Summary
MIS 11a and b	400–367	Decline in TANN to around 10 °C. Twin falls to a minimum of 0 °C at 398 ka BP. Tsum shows consistent decline to $\sim 20^\circ\text{C}$ at 397 ka BP. Precipitation parameters for MIS 11b, display a fall in precipitation around 380 ka BP. MAT and BRT suggest a progressive rise in precipitation from 400 ka BP culminating at 395 ka BP.
MIS 11c climatic optimum	427–400	Consistently high temperatures and precipitation. TANN ranges between 10 and 15 °C, indicating relative climatic stability. Three distinctive temperature peaks observed, with the third around 405 ka BP.
MIS 12/11 transition	433–427	Lowest annual temperatures ($\sim 5^\circ\text{C}$) before 430 ka BP. Brief temperature peak around 430 ka BP, followed by rapid return to cold conditions at 428 ka BP. Decline in precipitation until 430 ka BP, PANN ranging 400–600 mm. Transition to warmer, more humid climate around 428 ka BP with temperatures over 22 °C and annual precipitation rising to 600 mm.

413
 414
 415
 416



417

418 **Figure 3 – Comparison of the pollen-based quantitative reconstructions for MIS 11, (A)**
 419 **TANN and (B) PANN (BRT=red solid line; MAT=blue dotted line; WA-PLS=green dashed line), with other**
 420 **regional and global proxies: (C) $\delta^{18}O_G$ bulloides and (D) annual SSTs from function transfer of foraminiferal**
 421 **assemblages from ODP976 (Brice, 2007); (E) brGDGT-derived TANN from Tenaghi Philippon (Ardenghi**
 422 **et al., 2019); (F) PANN and (G) TANN from Lake Ohrid derived through the MAT method (Kousis et al.,**
 423 **2018); (H) Methane (CH_4) atmospheric concentrations (Loulergue et al., 2008) and (I) CO_2 atmospheric**
 424 **concentrations from Antarctic EPICA Dome C ice cores (Nehrbass-Ahles et al., 2020); (J) Atlantic $\delta^{18}O$**
 425 **(Voelker et al., 2010); (K) Summer insolation (Laskar et al., 2004); (L) Precession index and (M) Obliquity**
 426 **curve (Berger and Loutre, 1991). Orange band indicates the period encompassing the climatic optimum,**
 427 **and the blue bands highlight major millennial-scale climatic events.**



428

429 4.2.3 MIS 6–5 (133–80 ka BP)

430 The climatic reconstructions for the period between 133 and 128 ka BP, equivalent to the end of the MIS 6 glacial
431 period, also referred to as the penultimate glacial, indicate cold and dry conditions, though some differences
432 between methods are observed (Fig. 4). Generally, the three methods show low values of TANN (range of 10–
433 13°C) and Twin (range of -5°C to 3°C) for the glacial period (Fig. 4), but there appears to be disagreement in the
434 reconstruction of Tsum. While BRT and WA-PLS suggest an average Tsum of 20°C, which is already surprisingly
435 high, MAT indicates higher values (Fig. S4), which might be owed to the tendency of this method to overestimate
436 parameters as it is more sensitive than the other two methods and has been shown in other studies to have a wider
437 spread of estimates during glacial periods (Brewer *et al.*, 2008; Sinopoli *et al.*, 2019). On the other hand,
438 precipitation reconstructions seem to be relatively in agreement with each other, suggesting dry conditions with
439 PANN under 600mm. The results for this time period are also observed in other records and pollen-based
440 reconstructions from southern Europe and the Iberian margin (e.g. Sanchez Goñi *et al.*, 1999; Desprat *et al.*, 2005;
441 Brewer *et al.*, 2008; Sinopoli *et al.*, 2019; Leroy *et al.*, 2023).

442 The transition from MIS 6 to MIS 5 is characterised by a rise in temperature and precipitation indicative of a
443 gradually warmer and more humid climate. An increase in TANN is visible in all the three methods, from between
444 10–12 °C during the glacial to 12–15 °C at the beginning of MIS 5e, equivalent to the early Eemian (Fig. 4). This
445 reflects the shift from steppic taxa to *Quercus* and other temperate vegetation (Fig. S1) as was also recorded in
446 the marine records of MD952042 (Sanchez Goñi *et al.*, 1999) and MD01-2447 (Desprat *et al.*, 2007) from the
447 Iberian Margin. This progressive rise is paralleled by the rise in CO₂ and CH₄ from Antarctica, and the decrease
448 in δ¹⁸O (Desprat *et al.*, 2005; Voelker *et al.*, 2010; Oliveira *et al.*, 2016). However, this transition towards climatic
449 amelioration is interrupted by a short-lived event of abrupt cooling and drying, observed already in MIS 19 and
450 11. These events have previously been observed throughout the interglacials MIS 19, 11 and 5 in records from
451 the Iberian Margin (Sanchez Goñi *et al.*, 1999; Desprat *et al.*, 2007) and were considered to be events analogue
452 to Younger Dryas events or Heinrich-type events associated with the weakening of the AMOC during the
453 deglaciation period.

454 While there are some differences between the methods in terms of the specific timing of the peak climatic
455 optimum during the Eemian (something that is itself under particular debate in the literature, e.g. Sanchez Goñi
456 *et al.*, 1999), the reconstructions show that the highest temperatures (>15 °C) and humidity (≥600 mm) occurred
457 between 127–118 ka BP (Fig. 4, Tab. 4). This is coeval with the lightest isotopic δ¹⁸O signature from the Iberian
458 margin (Desprat *et al.*, 2007) and highest sea-surface temperatures recorded in cores ODP 977 in the Alboran sea
459 (Martrat *et al.*, 2004). During this climatic optimum, Tsum and Twin values peak with values higher than MIS 19
460 and 11 averaging >23 °C and 10 °C, respectively, indicating increased temperature during both winter and summer
461 months (Fig. S4). These parameters indicate a more humid and warmer climate during the optimum of the Eemian
462 than the present day, which corroborates the findings of several other studies in Europe (Guiot *et al.*, 1989;
463 Cheddadi *et al.* 1998; Sanchez Goñi *et al.*, 1999; Desprat *et al.*, 2007; Brewer *et al.*, 2008; Leroy *et al.*, 2023). For
464 example, reconstructions from Lake Ohrid, La Grande Pile, Les Echets and Le Bouchet also show a thermal
465 maximum around this time, between 127 and 118 ka, followed by cooling around 117 ka (Brewer *et al.*, 2008;
466 Sinopoli *et al.*, 2019).

467 Our results also match the findings by Brewer *et al.* (2008), who identified a difference between northern and
468 southern Europe, whereby records from higher latitudes experiences a sharp drop in temperatures and precipitation
469 following the optimum whereas the climate remained more stable conditions over a longer period in the south.
470 Our reconstructions for ODP 976, similarly to those from Lake Ohrid (Sinopoli *et al.*, 2019) and Lago di
471 Monticchio (Allen *et al.*, 1999; Brewer *et al.*, 2008), exhibit a gradual and continuous cooling trend without a
472 sudden decrease in temperatures and precipitation following the Eemian optimum, suggesting an intermediate
473 climate signal more similar to southern European sites than northern ones, and possibly corroborating the idea of
474 a weak latitudinal gradient during this period. However, our results for Psum and Pwin show that there was still
475 strong seasonality during the Eemian climate optimum at least in the Western Mediterranean, reflected more by
476 precipitation parameters than temperature (Fig. S4). During this period, our reconstructions show that, while the
477 climate was overall wetter than the glacial of MIS 6 (as well as the latter parts of the Eemian), the climatic optimum
478 was characterised by very dry summers and contrastingly wetter winters. This might be linked with a strong
479 Mediterranean climate during this time around the Alboran Sea, as previously suggested by Sanchez Goñi *et al.*
480 (1999) for the Iberian Margin.

481 The tail end of the optimum is characterised by a decrease in temperature and a rise in precipitation, visible
482 across all three methods, in agreement with other European records (Guiot *et al.*, 1989; Brewer *et al.*, 2008;
483 Sinopoli *et al.*, 2019). Throughout the rest of the interglacial, several fluctuations are observed between cool and
484 warm periods, also observed in other southern-European records, with counterparts in Atlantic δ¹⁸O records
485 (Sanchez Goñi *et al.*, 1999; Desprat *et al.*, 2007; Sinopoli *et al.*, 2019). Specifically, these occurred around 115
486 ka BP (Melisey I), 105 ka BP (St. Germain Ib) and around 87 ka BP (Melisey II), events which are characterised
487 by colonisation by *Cedrus* and steppic vegetation; these are alternated with temperate phases St. Germain Ia and

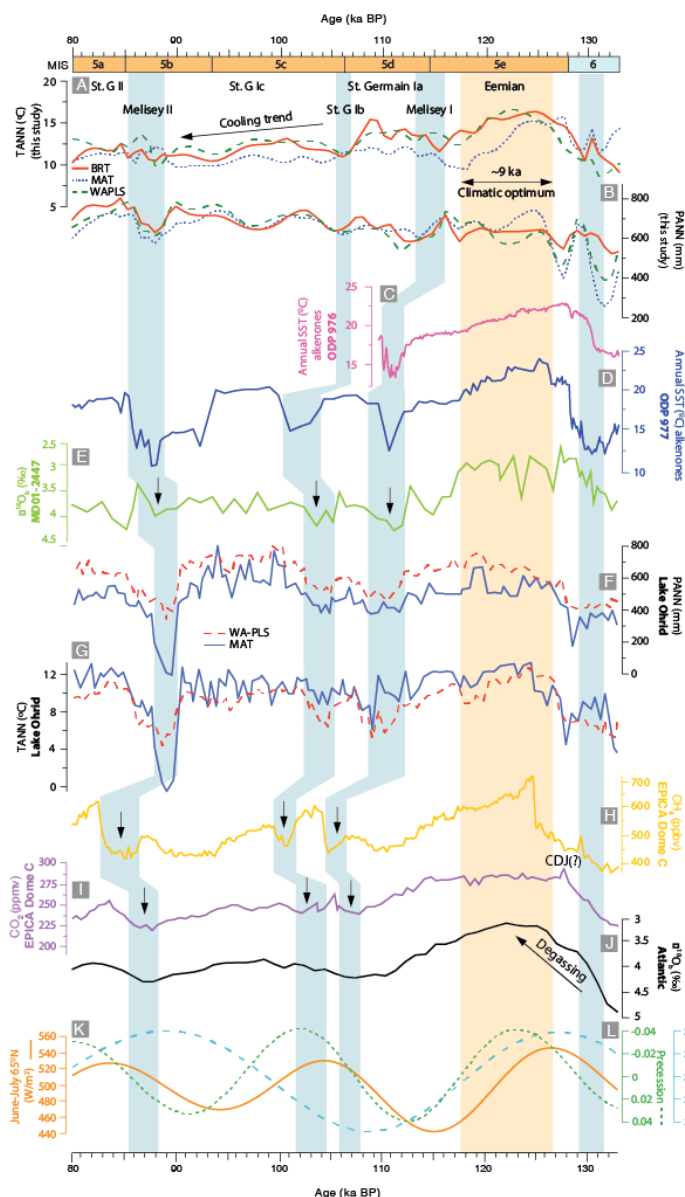


488 Ic, and St Germain II, during which heathlands and deciduous and Mediterranean forests expanded again (Sanchez
 489 Goñi *et al.*, 1999). These events correlate well with the first Dansgaard-Oeschger events (Dansgaard *et al.*, 1993),
 490 DO-25, 24 and 23 described by Masson-Delmotte *et al.* (2005). During this period of variability, our parameters
 491 suggest a progressive rise in precipitation and a slow decline in temperature throughout MIS 5c and the rest of the
 492 interglacial, consistent with climatic reconstructions from the Mediterranean such as Lake Ohrid (Sinopoli *et al.*,
 493 2019) and Lago di Monticchio (Brewer *et al.*, 2008; Sinopoli *et al.*, 2019), as well as records from the Iberian
 494 margin (Sanchez Goñi *et al.*, 1999; Desprat *et al.*, 2007) and eastern Mediterranean (Leroy *et al.*, 2023), showing
 495 similar trends throughout the Mediterranean. During MIS 5b, a notable drop in PANN is observed around 89–86
 496 ka BP, alongside a moderate rise in TANN. During substage 5a, both parameters decrease further, consistent with
 497 glacial inception of MIS 4 (Fig. 4).
 498

Table 4 - Summary of results of the pollen-based climatic reconstructions for MIS 6–5

Interval	Age (ka BP)	Summary
MIS 5a and b cooling	98–80	Drop in precipitation but a smaller rise in temperature around 89–86 ka BP. Parameters show a consistent decline in temperature during MIS 5a consistent with glacial inception moving towards MIS 4.
MIS 5c and d warm events	116–98	Progressive rise in precipitation and a slow decline in temperature during the rest of the interglacial.
Eemian (5e)	128–116	Highest temperatures (~15 °C) and humidity (≥600 mm) observed between 127–118 ka BP.
MIS 6/5 transition	133–128	Rise in temperature visible in all three methods. Temperature increases from 10–12 °C during the glacial to 12–15 °C at the onset of MIS 5.

499



500

501 **Figure 4 – Comparison of the pollen-based quantitative reconstructions from ODP976 for MIS 5, (A)**
 502 **TANN and (B) PANN (BRT=red solid line; MAT=blue dotted line; WA-PLS=green dashed line), with**
 503 **other regional and global proxies: (C) Alkenone SSTs from ODP976 (Martrat et al., 2014); (D) Alkenone**
 504 **SSTs from ODP977 (Martrat et al., 2004); (E) Benthic $\delta^{18}\text{O}$ from MD01-2447 (Desprat et al., 2007); (F)**
 505 **PANN and (G) TANN from Lake Ohrid derived through MAT and WAPLS (Sinopoli et al., 2019); (H)**
 506 **Methane (CH_4) atmospheric concentrations (Loulergue et al., 2008) and (I) CO_2 atmospheric**
 507 **concentrations from Antarctic EPICA Dome C ice cores (Nehrbass-Ahles et al., 2020); (J) Atlantic $\delta^{18}\text{O}$**
 508 **(Voelker et al., 2010); (K) Summer insolation (Laskar et al., 2004); (L) Precession index and (M)**
 509 **Obliquity curve (Berger and Loutre, 1991). Orange band indicates the period encompassing the climatic**
 510 **optimum, and the blue bands highlight major millennial-scale climatic events.**
 511



512 4.2.4 MIS 2–MIS1 (21 ka BP–present day)

513

514 Last Glacial Maximum to HE-1

515 During the Last Glacial Maximum (LGM), around 21–17.5 ka BP, MAT and WA-PLS suggest peculiarly high
516 TANN and Twin values, ranging between 12–15 °C and 0–10°C, respectively (Fig. 5, Tab. 5). MAT also suggests
517 drastically higher Tsum values during this period when compared with BRT and WA-PLS. This may once again
518 be due to the tendency of MAT to overestimate parameters during glacial periods, and is also linked to the inferior
519 reliability of WA-PLS when compared to the newer method BRT. Combourieu-Nebout *et al.* (2009) also noticed
520 that their MAT reconstruction for the end of the LGM were higher than expected and closer to present-day levels,
521 as it appears in the reconstruction methods of this current study. This discrepancy to the possible lack of good
522 present-day analogues for the cedar/heath pollen association which is dominant in the pollen record at the end of
523 the LGM (Combourieu-Nebout *et al.*, 2009). In contrast, BRT suggests relatively lower annual and seasonal
524 temperatures than the other two methods for the LGM period, which is more in line with previous interpretations
525 made by Combourieu-Nebout *et al.* (2009) on the basis the ODP Site 976 pollen record during this period. In their
526 study, TANN reconstructions suggested anomalies around -5°C and Twin between -10°C and -15°C. Overall,
527 precipitation during this period appears to be consistently low across all three methods, with PANN values
528 remaining below 600 mm/yr, indicating a dry climate in agreement with the previous study on the ODP 976 core
529 by Combourieu-Nebout *et al.* (2009), as well as the PANN reconstruction for the Padul record (Fig. 5) which
530 shows a period of low precipitation patterns between 20 and 16 ka BP consistent depleted δ_{DC31} values (Camuera
531 *et al.* 2018, 2019, 2022; García-Alix *et al.* 2021)

532 Between 17 and 15 ka BP, a drastic fall in temperature and precipitation is observed (Fig. 5). This change has
533 been previously attributed to the Oldest Dryas event in the south-western Mediterranean, consistent with Heinrich
534 Event 1 observed in several other marine and terrestrial records in the Mediterranean (Pons and Reille, 1988;
535 Watts *et al.*, 1996; Combourieu-Nebout *et al.*, 1998, 2002; Allen *et al.*, 2002; Peñalba *et al.*, 1997; Turon *et al.*,
536 2003; Naughton *et al.*, 2007; Fletcher and Sanchez Goñi, 2008; Bordon *et al.*, 2009) and has been interpreted as
537 increased dryness over the Alboran Sea (Combourieu *et al.*, 2009). Our climatic reconstructions suggest minimum
538 temperatures with Twin values of -5–0°C across all methods, and annual and seasonal precipitation values similar
539 to the late Pleniglacial with a minimum of ~300 mm shown by the MAT method. This event has a counterpart in
540 marine records for alkenone-derived SSTs from ODP Site 976 (Martrat *et al.*, 2014) and other Mediterranean sites
541 (Kallel *et al.*, 1997; Rohling *et al.*, 1998; Cacho *et al.*, 2001; Combourieu-Nebout *et al.*, 2002; Perez Folgado *et*
542 *al.*, 2003; Camuera *et al.*, 2021). Recent studies from the new Padul record found a similar pattern in their PANN
543 and TANN reconstructions (Camuera *et al.*, 2022; Rodrigo-Gámiz *et al.*, 2022), suggesting comparable conditions
544 over the Western Mediterranean during this period. This has also been corroborated by Ludwig *et al.*, (2018)
545 through model simulations of PANN and TANN over the Iberian Peninsula, which indicated a drastic decline in
546 both parameters during HE-1.

547

548 Lateglacial, beginning of MIS 1

549 A rise in temperature and precipitation is observed between 14.7 and 12.5 ka BP, shown consistently by the three
550 reconstruction methods (Fig. 5, Tab. 5). Although this is not reflected as strongly by the precipitation parameters,
551 temperature reconstructions achieved particularly with BRT and WA-PLS show two distinctive periods of
552 increased warmth centred around 14 and 13 ka BP, attributed respectively to the Bölling and Allerød (B-A) warm
553 interstadials (Zonneveld, 1996; Combourieu-Nebout *et al.*, 2009; Dormoy *et al.*, 2009; Camuera *et al.* 2019, 2021;
554 Rodrigo-Gamiz *et al.*, 2022). During these periods, Twin values ranging 0–6°C and TANN values of 12–14°C
555 (Fig. 5, Fig. S5). Precipitation reconstructions suggest similar seasonality to the present-day in the Mediterranean,
556 with wet winters and dry summers as evidenced by the increase in Pwin but relatively consistent Psum values (
557 Fig. S5). In comparison with the values reconstructed for the Holocene, temperatures during the B-A remain
558 slightly subdued (Fig. 5).

559 Between 12.5 and 11.7 ka BP, all three methods indicate a return to colder and drier conditions compared to
560 the B-A interstadial, related to the Younger Dryas event (YD). Twin values during the YD range from
561 approximately -2°C to 3°C, and TANN values range from 10°C to 13°C. Precipitation is also low across all three
562 methods, especially in PANN and Pwin, which decline from 700mm and 300mm during the B-A to 500mm and
563 250mm, respectively, during the YD. These results are similar to those reconstructed by Combourieu-Nebout *et*
564 *al.* (2009) but are slightly higher than the values reconstructed by Dormoy *et al.* (2009). A comparably colder and
565 more arid climate compared to the B-A in this region was also observed by Camuera *et al.* (2021, 2022) and by
566 Rodrigo-Gamiz *et al.* (2022), although their values were slightly higher for both parameters perhaps indicating a
567 slight difference on land within the Iberian Peninsula compared to the conditions in the Alboran Sea at this time.

568 Overall, however, our results show similar timings, trends and amplitudes to what has so far been observed in
569 regional records from the Mediterranean and Iberian Margin, and global proxies such as CH₄ records from
570 Antarctica (Jouzel *et al.*, 2007; Nehrbass-Ahles *et al.*, 2020).

571



572 Holocene

573 The transition from the YD to the Holocene at 11.7 ka BP is marked by an increase in temperature and precipitation
 574 parameters across all three methods (Fig. 5). TANN reaches similar levels to the present-day, and PANN reaches
 575 values above 600mm/yr. Seasonal temperature parameters Twin and Tsum show consistently high values with
 576 warmer summers and slightly cooler winters. There is a large difference between Psum and Pwin, indicating
 577 seasonal variation in wetness which may be related to the onset of present-day altitudinal vegetation belts and
 578 Mediterranean climate (Combourieu-Nebout *et al.*, 2009). This amelioration is coeval with the increase in SST
 579 values from ODP 976 which show warming in marine environments as well as on land at the beginning of the
 580 Holocene (Combourieu-Nebout *et al.*, 2002, 2009). This is also shown by alkenone and foraminiferal-based SST
 581 records in the nearby core MD 95-2042 (Cacho *et al.*, 2001; Perez Folgado *et al.*, 2003) and the $\delta^{13}\text{C}$ and $\delta^{18}\text{O}$
 582 depletion in the MD 90-917 core in the Adriatic Sea (Siani *et al.*, 2013).

583 Maximum temperatures and precipitation in our reconstructions mark the optimum climatic conditions of the
 584 Holocene between 9 and 7 ka BP, consistent with other studies in the Mediterranean (Bar-Matthews *et al.*, 1998;
 585 Rossignol-Strick, 1999; Kotthoff *et al.*, 2008; Ramos-Román *et al.* 2018, Marriner *et al.*, 2022), as well as in
 586 central Europe (Magny *et al.*, 2002; Martin *et al.*, 2020; Cartapanis *et al.*, 2022; d’Oliveira *et al.*, 2023). As shown
 587 by our Pwin and Psum values, seasonality is strong during this period—winter precipitation increases significantly
 588 (300 to 400 mm/yr) while summer precipitation reaches a minimum (around 50 mm/yr) suggesting strong seasonal
 589 contrasts. In the early Holocene, Twin values range from approximately -0.85 °C to 5.81 °C, while Tsum values
 590 range from 19.15 °C to 23.59 °C. These findings match the reconstructions by Dormoy *et al.* (2009) and Jalut *et al.*
 591 (2009) who suggested that in the Western and Central Mediterranean, the climatic optimum of the Holocene
 592 was characterised by hot and dry summers and wet and cool winters. This has also been corroborated by more
 593 recent climatic reconstructions for Padul (Ramos-Román *et al.*, 2018; Rodrigo-Gamiz *et al.*, 2022). This contrasts
 594 with results from Northern and Eastern Europe, where high year-round moisture and wet summers prevailed
 595 (Rossignol-Strick, 1999; Bar-Matthews *et al.*, 1998), consistent with the east-west precipitation gradient observed
 596 during the climatic optima of Holocene analogues.

597 The optimum is interrupted by a short-lived cooling event around 8.4–8.2 ka BP, observed in many other
 598 global records (Von Grafenstein *et al.*, 1998; Mayewski *et al.*, 2004; Alley and Agustsdottir, 2005; Pross *et al.*,
 599 2009; Marriner *et al.*, 2022). The reduction in our reconstructed parameters during the 8.2 ka event, particularly
 600 the reduction in precipitation although not as much in temperature, can be explained by a reduction in North
 601 Atlantic Deep Water (NADW) formation due to increased meltwater from the Laurentide lakes into the North
 602 Atlantic (Barber *et al.*, 1999; Ellison *et al.*, 2006).

603 The reconstructions for PANN indicate a generally decreasing trend for the last 7 ka with good consensus
 604 between methods (Fig. 6, Table 6). Meanwhile, TANN shows different amplitudes of change; while BRT and
 605 WAPLS indicate an overall upwards trend in temperatures between 6–2 ka BP, MAT suggests a comparatively
 606 more drastic decline. Short-term fluctuations previously identified by Combourieu-Nebout *et al.* (2009) and
 607 Dormoy *et al.* (2009) are also observed in our record around 6–5, 4.3 and 3.7 ka BP, which roughly correlate with
 608 Bond events in the North Atlantic (Bond *et al.*, 1997, 2001).

609 However, the climatic reconstructions from 7 ka onwards must be interpreted cautiously due to the increasing
 610 anthropogenic impact during this period. The decline in temperature and precipitation parameters, rather than
 611 being a result of progressive cooling, might in fact be an artificial result of increase in semi-desert taxa such as
 612 *Artemisia* and reduction in temperate and Mediterranean forest cover (Fig. S1) related to anthropogenic impact in
 613 the form of clearing (Combourieu-Nebout *et al.*, 2009). However, several other reconstructions for this period in
 614 this region (Camuera *et al.*, 2022; Rodrigo-Gamiz *et al.*, 2022; Liu *et al.*, 2023) and in Western Mediterranean (Di
 615 Rita *et al.*, 2022) suggest similar findings. Liu *et al.* (2023) proposed that the consistency of climate
 616 reconstructions during this period signifies that the changes observed are a reflection of regional climate rather
 617 than human activity in the form of agriculture or landscape modification and therefore should be considered as
 618 such. On the other hand, during the past 2 ka all methods indicate a substantial rise in temperatures and further
 619 decline in precipitation, most likely reflecting at this point the increasing human influence on vegetation
 620 composition, especially during the post-industrial era (Ruddiman *et al.*, 2016).

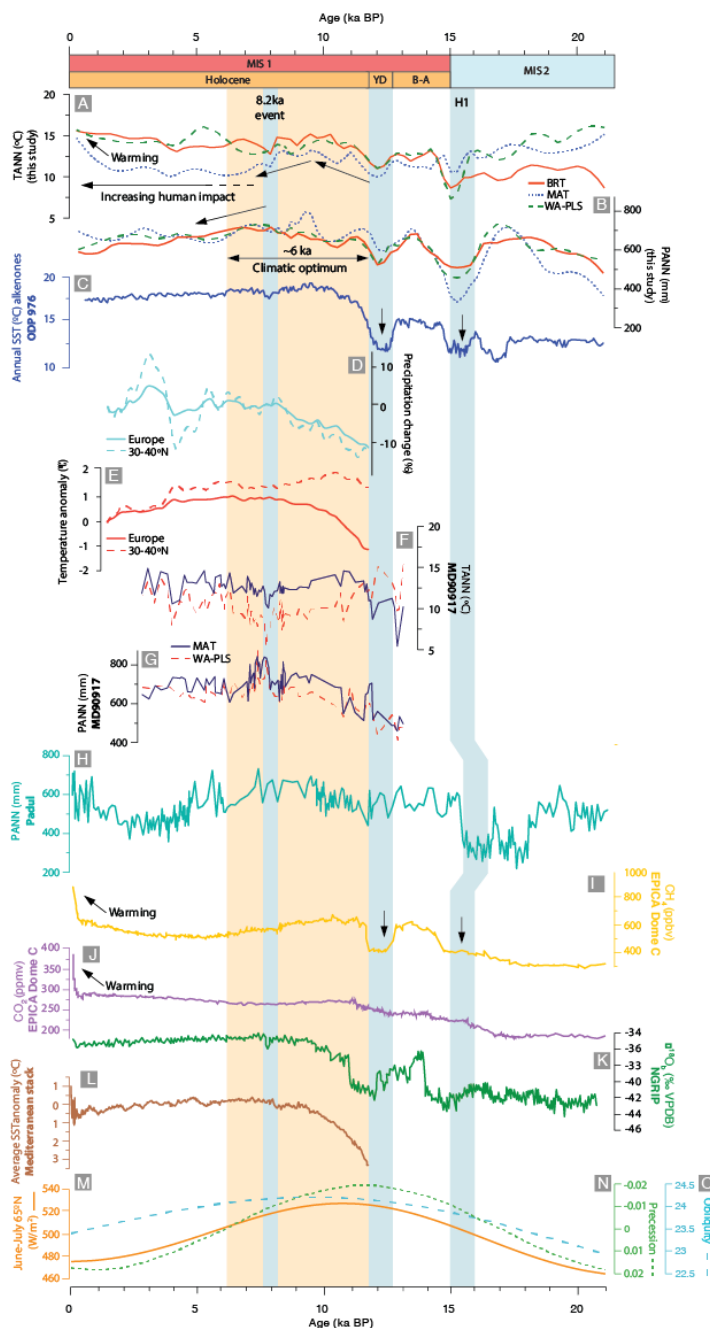
621

Table 5 - Summary of results of the pollen-based climatic reconstructions for MIS 2–1

Interval	Age (ka BP)	Summary
Middle-Late Holocene	6.4-present	BRT and WA-PLS indicate an overall upwards trend in temperatures. MAT suggests a comparatively more drastic decline.
Early-Middle Holocene climatic optimum	11.7-6.4	Consistent rise in temperature and precipitation by all three reconstructions. Climatic optimum observed between 11 and 7 ka BP All methods show a temperature rise above 13 °C, peak in precipitation reaching >700 mm. Interrupted by a noteworthy cold and dry event around 8.2 ka BP.



Younger Dryas	12.5-11.7	Return to colder and drier conditions Twin values during YD range from approximately -2°C to 3°C, and TANN values range from 10°C to 13°C. Precipitation is low across all three methods.
Bølling-Allerød	15-12.5	Temperature reconstructions show two distinctive periods of increased warmth. Attributed to Bølling and Allerød warm interstadials. Twin values ranging 0–6°C and TANN values of 12–14°C.
H1-Oldest Dryas	16-15	Drastic fall in temperature and precipitation observed, related to Oldest Dryas (H1) Climatic reconstructions suggest minimum temperatures with Twin values of -5–0°C. Annual and seasonal precipitation values similar to late Pleniglacial (~300 mm shown by MAT method).
MIS 2/1 transition	21.2-15	MAT and WA-PLS show high TANN ranging between 12–15 °C. PANN indicates a large range of 500–800 mm across the three methods. Significant drop in temperature and precipitation during H1; annual temperatures fall to 10–12 °C Precipitation falls below 600 mm (minimum ~300 mm shown by MAT).



622

623 **Figure 5 – Comparison of the pollen-based quantitative reconstructions from ODP976 for MIS 1, (A)**
 624 **TANN and (B) PANN (BRT=red solid line; MAT=blue dotted line; WA-PLS=green dashed line), with other**
 625 **regional and global proxies: (C) Alkenone SSTs from ODP976 (Martrat et al., 2014); (D) Precipitation**
 626 **change (%PANN) and (E) Temperature anomaly (TANN) for Europe from WAPLS (Herzschuh**
 627 **et al., 2023); (F) PANN and (G) TANN obtained through quantitative pollen-based reconstructions using**
 628 **MAT and WAPLS (Combourieu-Nebout et al., 2013); (H) Pollen-based quantitative reconstruction of**



629 **PANN from Padul derived using WAPLS (Camuera et al., 2023); (I) Methane (CH₄) atmospheric**
630 **concentrations (Louergue et al., 2008) and (J) CO₂ atmospheric concentrations from Antarctic EPICA**
631 **Dome C ice cores (Nehrbass-Ahles et al., 2020); (K) NGRIP ice δ¹⁸O (North Greenland Ice Core Project**
632 **Members, 2004); (L) Average SST anomaly from Mediterranean stack (Marriner et al., 2022); (M) Summer**
633 **insolation (Laskar et al., 2004); (N) Precession index and (O) Obliquity curve (Berger and Loutre, 1991).**
634 **Orange band indicates the period encompassing the climatic optimum, and the blue bands highlight major**
635 **millennial-scale climatic events.**

636

637 4.3 Interglacial analogues of the Holocene in the southwestern Mediterranean

638 The climate reconstructions show changes in temperature and precipitation in the Alboran Sea during MIS 19, 11,
639 5 and the Holocene (Fig. 6), which correlate with climatic changes observed in other regional and global proxies
640 indicating that overall the reconstructed parameters are reasonable and reliable. Our reconstructions enable a
641 valuable comparison of the structure and amplitude of millennial-scale climate variation during these periods in
642 the southwestern Mediterranean.

643 Before delving into a discussion about how MIS 19, 11 and 5 compare climatically and their suitability as
644 interglacial analogues of the Holocene, the implications of anthropogenic impact over the past 7 ka must be
645 considered. The extent to which humans have altered the current interglacial and therefore what is considered
646 ‘natural’ climate change has been subject of substantial debate over the past couple decades (Ruddiman, 2003,
647 2007; Ruddiman *et al.*, 2016). This is particularly with regard to the origin of the CO₂ increase by 20 ppmv, as
648 well as the rise in CH₄, during the late Holocene (Yin and Berger, 2015), believed to be a result of the clearing of
649 forests and agricultures over the past 7 ka BP. Ruddiman (2003, 2007) hypothesised, under what is known as the
650 early Anthropogenic hypothesis, that the rise in GHGs between 7 ka BP and the Industrial Era is not caused by
651 natural sources but rather by human intervention in the form of forest clearance, livestock domestication and
652 flooding of rice paddies (Ruddiman, 2003, 2007; Broecker and Stocker, 2006). The increase in GHGs resulting
653 from preindustrial farming was enough to cause anomalous warming and prolonged the duration of the
654 interglacial, whereas based on solar precession the Holocene would be expected to be nearing the end of its natural
655 course (Yin and Berger *et al.*, 2015). This hypothesis has significant implications on the reliability of comparisons
656 between MIS 1 and the interglacial analogues, and leads to significantly different conclusions about the natural
657 trajectory of the Holocene (Tzedakis, 2010). Some authors question the extent of anthropogenic impact on climate
658 during the pre-Industrial period altogether, making the debate over the early Anthropogenic hypothesis somewhat
659 irrelevant. Yin and Berger (2015) state that whether the hypothesis is right or wrong, the increase in CO₂ by 20
660 ppmv during the late Holocene is significantly smaller than the 120 ppmv released during the 20th and 21st
661 centuries, and therefore the late Holocene can be considered natural enough to enable comparisons with other
662 interglacials.

663 As shown in Figure 6, the MAT method suggests the latest warming trend has occurred over the last 2,000
664 years or so, while BRT and WA-PLS indicate a slower gradual warming over the past 4,000 years. This gradual
665 increase coincides with the gradual increase in GHGs evidenced by the CH₄ and CO₂ EPICA records, and these
666 also indicate that it is only in the most recent centuries that peak values are recorded, i.e. since the Industrial Era
667 (Jouzel *et al.*, 2007; Pol, 2010; Nehrbass-Ahles *et al.*, 2020). While the importance of human forcing on climate
668 is recognised, the idea that pre-Industrial activity represented a small enough contribution to GHG emissions is
669 still entertained to allow comparisons between the Holocene and Pleistocene interglacials.

670

671

672

673

674

675

676

677

678

679

680

681

682

683

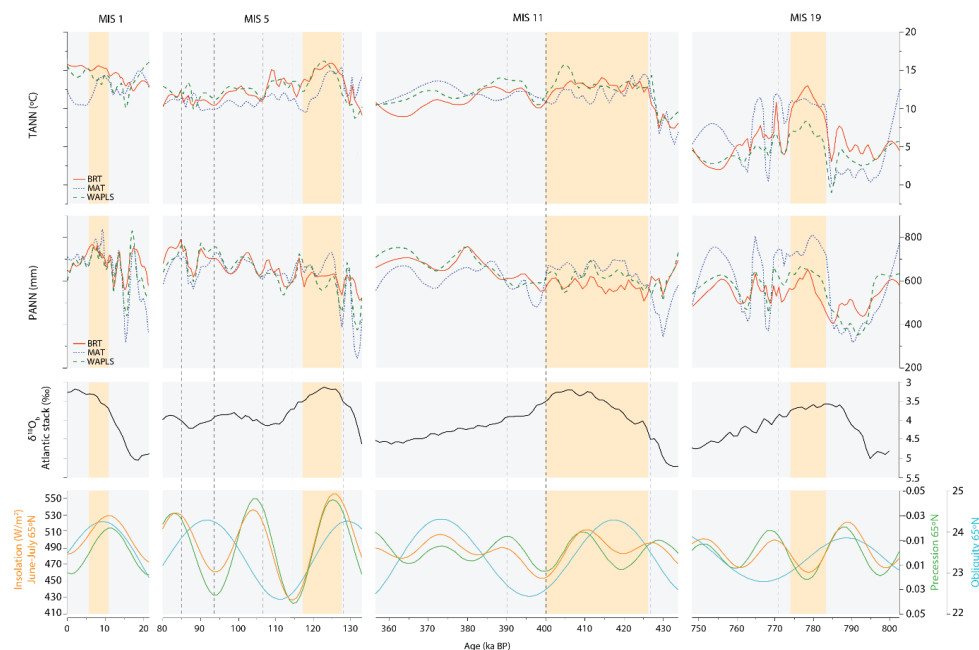
684

685

686

687

688



689
 690 **Figure 6 - Comparison of the quantitative pollen-based reconstructions (TANN and PANN) from ODP976**
 691 **for MIS 19, 11, 5 and 1, compared with the Atlantic $\delta^{18}\text{O}$ stack by Voelker et al. (2010) and solar orbital**
 692 **patterns: Summer insolation (Laskar et al., 2004), Precession index and Obliquity curve (Berger and**
 693 **Loutre, 1991). Orange bars indicate the period encompassing the climatic optimum in each interglacial.**
 694

695 The reconstructions for MIS 19 (Fig. 6) display the highest degree of variability throughout the interglacial,
 696 with high-amplitude fluctuations across all three methods between warm and colder substages. Generally, the
 697 models show a colder climate than the other interglacials (Fig. 6). These match the findings of other authors and
 698 it has been widely recognised that MIS 19 is colder than the interglacials after Termination V (Jouzel et al., 2007;
 699 Candy et al., 2014, 2024). When comparing to the EPICA records of MIS 19 to those of the other interglacials,
 700 the former shows lower concentrations of GHGs (Pol, 2010; Nehrbass-Ahles et al., 2020), supporting our findings
 701 of lower temperatures during this period. A colder climate than present during the climatic optimum of MIS 19c
 702 has been observed by Jouzel et al. (2007), who stated that this period was characterized by less pronounced
 703 warmth than interglacials MIS 5e, 7e, 9c, and 11c. Moreover, a main distinction between MIS 19 and the Holocene
 704 is that following the peak of MIS 19, temperatures decline relatively quickly, while during Holocene there is a
 705 short-lived decline in temperature, followed by a renewed increase and stabilisation during the Late Holocene
 706 (Candy et al., 2014). In general, while the solar forcing of MIS 19 might be more similar to MIS 1, the climatic
 707 structure of MIS 19 has little resemblance to MIS 1 when considering the duration of the sustained warmth during
 708 the pre-Industrial Holocene, at least in the region around the Alboran Sea.

709 MIS 11 differs from MIS 19 in the magnitude of temperature variations. It is also much longer than both MIS
 710 19 and MIS 5, and indeed the Holocene, due to its unique antiphasing between insolation and obliquity (Ruddiman
 711 et al., 2007; Nomade et al. 2019; Tzedakis, 2010; Tzedakis et al., 2022). While MIS 11 exhibits warmer
 712 temperatures compared to MIS 19, it still shows some degree of variability as observed with its high- and
 713 moderate-intensity climatic variability events and climatic fluctuations during the optimum, like the OHO.
 714 Overall, however, it is significantly more stable than MIS 19. According to Candy et al. (2014), if the early
 715 Anthropogenic hypothesis is not accepted, MIS 11c is a closer climatic analogue, which means that the current
 716 interglacial may last for over 50 ka (Loutre and Berger, 2003; McManus et al., 2003; Candy et al., 2014). If
 717 instead this hypothesis is accepted then MIS 19 and MIS 1 become more similar, meaning that the current
 718 interglacial would be close to its end if it weren't for anthropogenic forcing (Candy et al., 2014; Tzedakis, 2010).
 719 The key particularity of accepting MIS 11 as an analogue is that it is the only interglacial with a combination of
 720 elevated GHG concentrations and an extended duration. Considering that human activity is affecting the length
 721 of the Holocene (Tzedakis et al., 2012; IPCC 2022), this makes MIS 11c an important analogue for how the earth's
 722 climatic system functions under extended interglacial conditions (Candy et al., 2014, 2024).



723 Similarly to MIS 11, MIS 5 is characterised by elevated greenhouse gas levels and high sea levels, although
724 this interglacial has been criticised as an analogue by previous authors due to its high-amplitude fluctuations in
725 solar forcing. The reconstructions for MIS 5, particularly for MIS 5e (the Eemian), suggest a significantly warmer
726 climate regime compared with the other interglacial analogues. In terms of duration, MIS 5e is slightly shorter
727 than MIS 19, but similarly to MIS 11 it exhibits more stable climatic conditions as also corroborated by the lower
728 variation in SSTs in records from the Western Mediterranean (Martrat *et al.*, 2004). A warmer climate than other
729 interglacial analogues and the Holocene (specifically, warmer than pre-Industrial levels) has been previously
730 observed for the Eemian, for example at Padul (Camuera *et al.*, 2019), La Grande Pile (Guiot *et al.* 1989; Brewer
731 *et al.*, 2008) and in the North Atlantic (Zhuravleva, 2018). On a global average, MIS 5e has been found to be the
732 warmest interglacial of the past 800 kyr (Tzedakis *et al.*, 2022). When considering the factors together, i.e.
733 significantly higher temperatures, short duration, and high-amplitude fluctuations in solar forcing, in the case of
734 our reconstructions MIS 5 appears to be the least suitable analogue when compared with MIS 19 and 11.

735 Our high-resolution climatic reconstructions have demonstrated that in terms of magnitude of warmth,
736 structure, stability and duration the interglacial analogues of the Holocene are, fundamentally, unique. Although
737 they all are reoccurring events and share similar patterns such as the abrupt shifts from glacial to interglacial, the
738 occurrence of climatic optimums soon after the transition, and cold events and Younger-Dryas-like events, the
739 associated climate feedbacks in each interglacial produce very different climatic histories that are difficult to
740 compare with the Holocene. As Candy *et al.* (2014) point out, there is no reason to expect that the climate of MIS
741 1 should naturally follow the pattern of MIS 11 or 19 or indeed MIS 5, despite the close similarities in insolation
742 forcing, greenhouse gas concentration and temperatures. The study of past interglacials does not offer a direct
743 blueprint for predicting the future evolution of the Holocene. However, these interglacial analogues are valuable
744 for exploring the responses of the Earth's processes under different forcing factors which closely resemble the
745 climate system during the Holocene. What emerges from the climatic reconstructions from ODP Site 976 and the
746 close comparisons with global and regional records is that this site is extremely sensitive to global changes which
747 in turn can be used to infer that the southwestern Mediterranean will be highly susceptible to future climate change
748 and anthropogenic forcing.

749 **5. Conclusion**

750 This study has provided valuable insights into the climatic variations during MIS 19, 11, 5 and 1, within the
751 southwestern Mediterranean region. Through pollen-based climatic reconstructions, we have established
752 correlations between temperature and precipitation changes in our study area with those observed in other regional
753 and global proxies, confirming the reliability of our findings. These reconstructions facilitate a comprehensive
754 comparison of millennial-scale climate variations during these interglacials, shedding light on their unique
755 climatic structures and amplitudes.

756 The reconstructions highlight a temperature increase from MIS 19 to the Holocene and distinct climatic
757 characteristics of each interglacial period. MIS 19 exhibits high variability and colder temperatures compared to
758 subsequent interglacials and the Holocene. Conversely, MIS 11 displays warmer temperatures and greater
759 stability, offering an insight into interglacials of prolonged duration, crucial when considering that the
760 anthropogenically-driven warming of the post-Industrial era might be artificially prolonging the current
761 interglacial. Reconstructions for MIS 5 suggested overall warmer conditions, especially during the Eemian, but
762 this higher temperature coupled with high-amplitude fluctuations in solar forcing makes it a less suitable Holocene
763 analogue.

764 While past interglacials do not provide a straightforward blueprint for predicting the future evolution of MIS
765 1, they offer invaluable insights into Earth's responses to different forcing factors during periods with similar
766 climatic conditions to the Holocene. The pollen-based climatic reconstructions for MIS 19, 11 and 5 serve as
767 crucial benchmarks for understanding the sensitivity of the southwestern Mediterranean to global changes, and
768 underscore the importance of mitigating climate change in this region.

769 **Competing interests**

770 At least one of the (co-)authors is a member of the editorial board of *Climate of the Past*.

771 **Acknowledgments**

772 We sincerely appreciate the financial support from the ANR project Neandroots (Agence Nationale de la
773 Recherche, project No. ANR-19-CE27-0011-01), the Muséum national d'Histoire naturelle (MNHN), and the
774 Centre National de la Recherche Scientifique (CNRS). apThanks to the ISEM, the Institut des Sciences de
775 l'Évolution de Montpellier, UMR CNRS 5554 ISEM (Université de Montpellier) for hosting D. Sassoon on
776 multiple occasions for training on transfer functions. Special thanks to Léa d'Oliveira for the assistance with the
777 transfer function models and for her help troubleshooting the scripts. This is an ISEM contribution number
778 XXX (tbc).

779



783 **Supplementary data**

784 Supplementary data to this article can be found online at <https://data.mendeley.com/datasets/m4kzgwk6b9/1>

785

786 **References**

- 787 Allen, J. R. M., Watts, W. A., McGee, E., and Huntley, B.. Holocene environmental variability – the record from
788 Lago Grande di Monticchio, Italy, *Quatern. Int.*, 88, 69–80, 2002.
- 789 Allen, J.R.M., Huntley, B., Brandt, U., Brauer, A., Hubberten, H., Keller, J., Kraml, M., Mackensen, A., Mingram,
790 J., Negendank, J.F.W., Nowaczyk, N.R., Oberhansli, H., Watts, W.A., Wulf, S., Zolitschka, B. Rapid
791 environmental changes in southern Europe during the last glacial period. *Nature* 400, 740e743. <https://doi.org/10.1038/23432>, 1999.
- 792 Alley, R.B., Agustsdottir, A.M. The 8k event: cause and consequences of a major Holocene abrupt climate change.
793 *Quat Sci Rev.* 24, 1123–1149, 2005.
- 794 Alonso, B., Ercilla, G., Martínez-Ruiz, F., Baraza, J., and Galimont, A. Pliocene-Pleistocene sedimentary facies
795 at Site 976: Depositional history in the northwestern Alboran Sea. *Proc Integr Ocean Drill Program*,
796 161(1994), 57–68. <https://doi.org/10.2973/odp.proc.sr.161.206>, 1999.
- 797 Ardenghi, N., Mulch, A., Koutsodendris, A., Pross, J., Kahmen, A., and Niedermeyer, E. M. Temperature and
798 moisture variability in the eastern Mediterranean region during Marine Isotope Stages 11–10 based on
799 biomarker analysis of the Tenaghi Philippon peat deposit. *Quat Sci Rev.* 225,
800 <https://doi.org/10.1016/j.quascirev.2019.105977>, 2019.
- 801 Azibeiro, L. A., Sierro, F. J., Capotondi, L., Lirer, F., Andersen, N., González-Lanchas, A., Alonso-Garcia, M.,
802 Flores, J. A., Cortina, A., Grimalt, J. O., Martrat, B., and Cacho, I. Meltwater flux from northern ice-sheets to
803 the Mediterranean during MIS 12. *Quat Sci Rev.* 268. <https://doi.org/10.1016/j.quascirev.2021.107108>, 2021.
- 804 Bar-Matthews, M., Ayalon, A., and Kaufman, A. *Middle to late Holocene (6500 yr period) paleoclimate in the*
805 *Eastern Mediterranean region from stable isotopic composition of speleothems from Soreq Cave, Israel*, in:
806 *Environment and society in times of climate change*, edited by: Issar, A. and Brown, N., Kluwer Academic,
807 Dordrecht, 203–214, 1998.
- 808 Barber, D.C., Dyke, A., Hillaire-Marcel, C., Jennings, A.E., Andrews, J.T., Kerwin, M.W., Bilodeau, G.,
809 McNeely, R., Southon, J., Morehead, M.D., and Gagnon, J.M. Forcing of the cold event of 8,200 years ago by
810 catastrophic drainage of Laurentide lakes. *Nature*, 400(6742), pp.344-348, 1999.
- 811 Barbero, M., Quézel, P., Rivas-Martínez, S. Contribution à l'étude des groupements forestiers et préforestiers du
812 Maroc. *Phytocoenologia* 9, pp.311–412, 1981.
- 813 Bauch, H.A., Erlenkeuser, H., Helmke, J.P., Struck, U. A paleoclimatic evaluation of marine oxygen isotope stage
814 11 in the high-northern Atlantic (Nordic seas). *Glob. Planet. Change*, 24, 27e39.
815 [https://doi.org/10.1016/S0921-8181\(99\)00067-3](https://doi.org/10.1016/S0921-8181(99)00067-3), 2000.
- 816 Benabid, A. Bref aperçu sur la zonation altitudinale de la végétation climatique du Maroc, *Ecol. Medit.*, 8(1–2),
817 pp.301–315, 1982.
- 818 Berger, A., and Loutre, M.F. *Climate 400,000 years ago, a key to the future?* In: A.W. Droxler, R.Z. Past
819 Interglacials Working Group of Pages, Interglacials of the last 800,000 years. *R. of Geop.*, 54, pp.162-219,
820 2003.
- 821 Berger, A., and Loutre, M.F. An exceptionally Long Interglacial Ahead? *Science* 297, 1287–1288.
822 [doi:10.1126/science.1076120](https://doi.org/10.1126/science.1076120), 2002.
- 823 Bertini, A., Toti, F., Marino, M., Ciaranfi, N. Vegetation and climate across the early-middle Pleistocene transition
824 at the Montalbano Jonico section (southern Italy). *Quat Int.* 383, 74-88, 2015.
- 825 Blain, H. A., Fagoaga, A., Ruiz-Sánchez, F. J., García-Medrano, P., Ollé, A., and Jiménez-Arenas, J. M. Coping
826 with arid environments: A critical threshold for human expansion in Europe at the Marine Isotope Stage 12/11
827 transition? The case of the Iberian Peninsula. *J. Hum. Evol.* 153. <https://doi.org/10.1016/j.jhevol.2021.102950>,
828 2021.
- 829 Bond, G., Kromer, B., Beer, J., Muscheler, R., Evans, M.N., Showers, W., Hoffmann, S., Lotti-Bond, R., Hajdas,
830 I., and Bonani, G. Persistent solar influence on North Atlantic climate during the Holocene. *Science* 278, 1257-
831 1266, 2001.
- 832 Bond, G., Showers, W., Cheseby, M., Lotti, R., Almasi, P., de Menocal, P., Priore, P., Cullen, H., Hajdas, I., and
833 Bonani, G. A pervasive millennial-scale cycle in the North Atlantic Holocene and glacial climates. *Science*
834 294, 2130-2136, 1997.
- 835 Bordon, A., Peyron, O., Lézine, A.-M., Brewer, S., and Fouache, E. Pollen-inferred Late-Glacial and Holocene
836 climate in southern Balkans (Lake Maliq), *Quatern. Int.*, 200, 19–30, 2009.
- 837 Brewer, S., Guiot, J., Sánchez-Goñi, M.F., and Klotz, S. The climate in Europe during the Eemian: a multi-method
838 approach using pollen data. *Quat Sci Rev.* 27(25-26), pp.2303-2315, 2008.
- 839 Brice, R. *Variabilité Climatique en Mer d'Alboran au cours de la Teminaison V (MIS 12/11)*. Unpublished thesis,
840 University of Bordeaux, 2007.
- 841



- 842 Broecker, W. S., and Stocker, T. L.: The Holocene CO₂ rise. Anthropogenic or natural? *Eos, Trans. Am. Geophys.*
843 *Union*, 87(3), 27. doi:10.1029/2006EO030002, 2006.
- 844 Bulian, F., Kouwenhoven, T. J., Jiménez-Espejo, F. J., Krijgsman, W., Andersen, N., and Sierro, F. J. Impact of
845 the Mediterranean-Atlantic connectivity and the late Miocene carbon shift on deep-sea communities in the
846 Western Alboran Basin. *Palaeogeogr. Palaeoclimatol. Palaeoecol.*, 589.
847 <https://doi.org/10.1016/j.palaeo.2022.110841>, 2022.
- 848 Cacho, I., Grimalt, J. O., Canals, M., Sbaiffi, L., Shackleton, N., Schönfeld, J., and Zahn, R. Variability of the
849 western Mediterranean Sea surface temperature during the last 25,000 years and its connection with the
850 northern hemisphere climatic changes. *Paleoceanography*, 16, 40–52, 2001.
- 851 Cacho, I., Grimalt, J.O., Sierro, F.J., Shackleton, N., Canals, M. Evidence for enhanced Mediterranean
852 thermohaline circulation during rapid climatic coolings. *Earth Planet Sci Lett*, 183, 417–429, 2000.
- 853 Camuera, J., Jiménez-Moreno, G., Ramos-Román, M.J., García-Alix, A., Toney, J.L., Anderson, R.S., Jiménez-
854 Espejo, F., Bright, J., Webster, C., Yanes, Y., and Carrión, J.S. Vegetation and climate changes during the last
855 two glacial-interglacial cycles in the western Mediterranean: a new long pollen record from Padul (southern
856 Iberian Peninsula). *Quat Sci Rev*, 205, pp.86-105, 2019.
- 857 Camuera, J., Jiménez-Moreno, G., Ramos-Román, M.J., García-Alix, A., Toney, J.L., Anderson, R.S., Jiménez-
858 Espejo, F., Kaufman, D., Bright, J., Webster, C., and Yanes, Y. Orbital-scale environmental and climatic
859 changes recorded in a new ~ 200,000-year-long multiproxy sedimentary record from Padul, southern Iberian
860 Peninsula. *Quat Sci Rev*, 198, pp.91-114, 2018.
- 861 Camuera, J., Jiménez-Moreno, G., Ramos-Román, M.J., García-Alix, A., Jiménez-Espejo, F.J., Toney, J.L., and
862 Anderson, R.S. Chronological control and centennial-scale climatic subdivisions of the Last Glacial
863 Termination in the western Mediterranean region. *Quat Sci Rev*, 255, p.106814, 2021.
- 864 Camuera, J., Ramos-Román, M.J., Jiménez-Moreno, G., García-Alix, A., Ilvonen, L., Ruha, L., Gil-Romera, G.,
865 González-Sampérez, P., and Seppä, H. Past 200 kyr hydroclimate variability in the western Mediterranean and
866 its connection to the African Humid Periods. *Sci. Rep.*, 12(1), p.9050, 2022.
- 867 Candy, I., Schreve, D. C., Sherriff, J., and Tye, G. J. Marine Isotope Stage 11: Palaeoclimates, palaeoenvironments
868 and its role as an analogue for the current interglacial. *Earth-Sci Rev*, 128, 18–51.
869 <https://doi.org/10.1016/j.earscirev.2013.09.006>, 2014.
- 870 Candy, I., Oliveira, D., Parkes, D., Sherriff, J., and Thornalley, D. Marine Isotope Stage 11c in Europe: Recent
871 advances in marine–terrestrial correlations and their implications for interglacial stratigraphy—a review.
872 *Boreas*, 2024.
- 873 Cartapanis, O., Jonkers, L., Moffa-Sanchez, P., Jaccard, S.L., and de Vernal, A. Complex spatio-temporal
874 structure of the Holocene Thermal Maximum. *Nat. Commun.*, 13(1), p.5662, 2022.
- 875 Cheddadi, R., Lamb, H.F., Guiot, J., and van der Kaars, S. Holocene climatic change in Morocco: a quantitative
876 reconstruction from pollen data. *Climate dynamics*, 14, 883–890, 1998.
- 877 Chevalier, M., Davis, B. A. S., Heiri, O., Seppä, H., Chase, B. M., Gajewski, K., Lacourse, T., Telford, R. J.,
878 Finsinger, W., Guiot, J., Kühl, N., Maezumi, S. Y., Tipton, J. R., Carter, V. A., Brussel, T., Phelps, L. N.,
879 Dawson, A., Zanon, M., Vallé, F., ... Kupriyanov, D. Pollen-based climate reconstruction techniques for late
880 Quaternary studies. *Earth-Sci Rev*, 210, 103384. <https://doi.org/10.1016/j.earscirev.2020.103384>, 2020.
- 881 Combourieu-Nebout, N., Bertini, A., Russo-Ermolli, E., Peyron, O., Klotz, S., Montade, V., Fauquette, S., Allen,
882 J., Fusco, F., Goring, S., Huntley, B., Joannin, S., Lebreton, V., Magri, D., Martinetto, E., Orain, R., and
883 Sadori, L. Climate changes in the central Mediterranean and Italian vegetation dynamics since the Pliocene.
884 *Rev. Palaeobot. Palynol.* 218, 127–147, 2015.
- 885 Combourieu-Nebout, N., Londeix, L., Baudin, F., Turon, J.-L., von Grafenstein, R., and Zahn, R. *Quaternary
886 marine and continental paleoenvironments in the western Mediterranean (Site 976, Alboran Sea):
887 palynological evidence*, in: Proc. ODP Sci. Results, 161: College Station, TX (Ocean Drilling Program), edited
888 by: Zahn, R., Comas, M. C., and Klaus, A., pp.457–468, 1999.
- 889 Combourieu-Nebout, N., Paterne, M., Turon, J. L., and Siani, G. A high-resolution record of the last deglaciation
890 in the Central Mediterranean Sea: Palaeovegetation and Palaeohydrological evolution, *Quat Sci Rev*, 17, 303–
891 317, 1998.
- 892 Combourieu-Nebout, N., Peyron, O., Bout-Roumazeille, V., Goring, S., Dormoy, I., Joannin, S., Sadori, L., Siani,
893 G., and Magny, M. Holocene vegetation and climate changes in central Mediterranean inferred from a high-
894 resolution marine pollen record (Adriatic Sea). *Clim. Past* 9, 2023–2042, 2013.
- 895 Combourieu-Nebout, N., Peyron, O., Dormoy, I., Desprat, S., Beaudouin, C., Kotthoff, U., and Marret, F. Rapid
896 climatic variability in the west Mediterranean during the last 25,000 years from high resolution pollen data.
897 *Clim. Past*, 5(3), 503–521. <https://doi.org/10.5194/cp-5-503-2009>, 2009.
- 898 Combourieu-Nebout, N., Turon, J. L., Zahn, R., Capotondi, L., Londeix, L., and Pahnke, K. Enhanced aridity and
899 atmospheric high-pressure stability over the western Mediterranean during the North Atlantic cold events of
900 the past 50 k.y. *Geology*, 30(10), 863–866. [https://doi.org/10.1130/0091-
901 7613\(2002\)030<0863:EAHAHP>2.0.CO;2](https://doi.org/10.1130/0091-7613(2002)030<0863:EAHAHP>2.0.CO;2), 2002.



- 902 d'Oliveira, L., Dugerdil, L., Ménot, G., Evin, A., Muller, S.D., Ansanay-Alex, S., Azuara, J., Bonnet, C., Bremond,
903 L., Shah, M., and Peyron, O. Reconstructing 15,000 years of southern France temperatures from coupled
904 pollen and molecular (brGDGT) markers (Canroute, Massif Central). *Clim. Past* 19, 2127–2156.
905 <https://doi.org/10.5194/cp-19-2127-2023>, 2023.
- 906 Dansgaard, W., Johnsen, S.J., Clausen, H.B., Dahl-Jensen, D., Gundestrup, N.S., Hammer, C.U., Hvidberg, C.S.,
907 Steffensen, J.P., Sveinbjörnsdóttir, A.E., Jouzel, J., Bond, G. Evidence for general instability of past climate
908 from a 250-kyr ice-core record. *Nature* 364, 218–220, 1993.
- 909 Davis, B. A. S., Brewer, S., Stevenson, A. C., Guiot, J. The temperature of Europe during the Holocene
910 reconstructed from pollen data. *Quat Sci Rev*, 22, 1701–1716, 2003.
- 911 De'ath, G. Boosted trees for ecological modeling and prediction. *Ecology* 88, 243–251.
912 [https://doi.org/10.1890/0012-9658\(2007\)88\[243:BTfEMA\]2.0.CO;2](https://doi.org/10.1890/0012-9658(2007)88[243:BTfEMA]2.0.CO;2), 2007.
- 913 Desprat, S., Combourieu-Nebout, N., Essallami, L., Sicre, M.A., Dormoy, I., Peyron, O., Siani, G., Bout
914 Roumazeilles, V., Turon, J.L. Deglacial and Holocene vegetation and climatic changes at the southernmost tip
915 of the Central Mediterranean from a direct land–sea correlation. *Clim. Past* 9, 767–787, 2013.
- 916 Desprat, S., Sánchez Goñi, M. F., Naughton, F., Turon, J. L., Duprat, J., Malaizé, B., Cortijo, E., Peyrouquet, J.
917 P. Climate variability of the last five isotopic interglacials: Direct land-sea-ice correlation from the multiproxy
918 analysis of North-Western Iberian margin deep-sea cores. *Developments in Quaternary Science*, 7(C), pp.375–
919 386. [https://doi.org/10.1016/S1571-0866\(07\)80050-9](https://doi.org/10.1016/S1571-0866(07)80050-9), 2007.
- 920 Desprat, S., Sánchez Goñi, M. F., Turon, J. L., McManus, J. F., Loutre, M. F., Duprat, J., Malaizé, B., Peyron, O.,
921 Peyrouquet, J. P. Is vegetation responsible for glacial inception during periods of muted insolation changes?
922 *Quat Sci Rev*, 24(12–13), pp.1361–1374. <https://doi.org/10.1016/j.quascirev.2005.01.005>, 2005.
- 923 Di Rita, F., Ghilardi, M., Fagel, N., Vacchi, M., Warichet, F., Delanghe, D., Sicurani, J., Martinet, L., Robresco,
924 S. Natural and anthropogenic dynamics of the coastal environment in northwestern Corsica (western
925 Mediterranean) over the past six millennia. *Quat Sci Rev*, 278, p.107372, 2022.
- 926 Donders, T., Panagiotopoulos, K., Koutsodendrís, A., Bertini, A., Mercuri, A.M., Masi, A., Combourieu-Nebout,
927 N., Joannin, S., Kouli, K., Kousis, I., Peyron, O. 1.36 million years of Mediterranean forest refugium dynamics
928 in response to glacial–interglacial cycle strength. *PNAS*, 118(34), p.e2026111118, 2021.
- 929 Dormoy, I., Peyron, O., Combourieu-Nebout, N., Goring, S., Kotthoff, U., Magny, M., Pross, J. Terrestrial climate
930 variability and seasonality changes in the Mediterranean region between 15,000 and 4,000 years BP deduced
931 from marine pollen records. *Clim. Past* 5, 615–632. <https://doi.org/10.5194/cp-5-615-2009>, 2009.
- 932 Dugerdil, L., Joannin, S., Peyron, O., Jouffroy-Bapicot, I., Vannière, B., Boldgiv, B., Unkelbach, J., Behling, H.,
933 Ménot, G. Climate reconstructions based on GDGT and pollen surface datasets from Mongolia and Baikal
934 area: calibrations and applicability to extremely cold–dry environments over the Late Holocene. *Clim. Past*,
935 17(3), pp.1199–1226, 2021.
- 936 Ellison, C.R., Chapman, M.R., Hall, I.R. Surface and deep ocean interactions during the cold climate event 8,200
937 years ago. *Science*, 312(5782), pp.1929–1932, 2006.
- 938 Elith, J., Leathwick, J. R., Hastie, T. A working guide to boosted regression trees. *J. Anim. Ecol.*, 77(4), 802–813,
939 2008.
- 940 Fletcher W., Sanchez Goñi M.F. Orbital- and sub-orbital-scale climate impacts on vegetation of the western
941 Mediterranean basin over the last 48,000 yr. *Quat. Res.*, 70(3), 451–464, 2008.
- 942 García-Alix, A., Camuera, J., Ramos-Román, M.J., Toney, J.L., Sachse, D., Schefuß, E., Jiménez-Moreno, G.,
943 Jiménez-Espejo, F.J., López-Avilés, A., Anderson, R.S., Yanes, Y. Paleohydrological dynamics in the
944 Western Mediterranean during the last glacial cycle. *Glob. Planet. Change*, 202, p.103527, 2021.
- 945 Giaccio, B., Regattieri, E., Zanchetta, G., Nomade, S., Renne, P.R., Sprain, C.J., Drysdale, R.N., Tzedakis, P.C.,
946 Messina, P., Scardia, G., Sposato, A. Duration and dynamics of the best orbital analogue to the present
947 interglacial. *Geology*, 43(7), 603–606, 2015.
- 948 Gironé, A., Maiorano, P., Marino, M., Kucera, M. Calcareous plankton response to orbital and millennial-scale
949 climate changes across the Middle Pleistocene in the western Mediterranean. *Palaeogeogr. Palaeoclimatol.*
950 *Palaeoecol.*, 392, 105–116. <https://doi.org/10.1016/j.palaeo.2013.09.005>, 2013.
- 951 Gonzalez-Donoso, J.M., Serrano, F., Linares, D. Sea surface temperature during the Quaternary at ODP Sites 976
952 and 975 (western Mediterranean). *Palaeogeogr. Palaeoclimatol. Palaeoecol.* 162, 17–44, 2000.
- 953 Grafenstein, U., Erlenkeuser, H., Brauer, A., Jouzel, J., Johnsen, S.J. A mid-European decadal isotope-climate
954 record from 15,500 to 5000 years BP. *Science*, 284(5420), 1654–1657, 1999.
- 955 Grieser, J., Giommes, R., Bernardi, M. New LocClim – the Local Climate Estimator of FAO, *Geophysical*
956 *research abstracts*, 8, 08305, 2006.
- 957 Guiot, J., Cramer, W. Climate Change: The 2015 Paris Agreement Thresholds and Mediterranean Basin
958 Ecosystems. *Science*, 354, 465–468, 2016.
- 959 Guiot, J. Methodology of the last climatic reconstruction in France from pollen data. *Palaeogeogr.*
960 *Palaeoclimatol. Palaeoecol.* 80, 49–69, 1990.



- 961 Guiot, J., Pons, A., de Beaulieu, J.-L., Reille, M. A 140,000 year continental climate reconstruction from two
962 European pollen records. *Nature* 338, 309-313, 1989.
- 963 Herzsich, U., Böhmer, T., Chevalier, M., Hébert, R., Dallmeyer, A., Li, C., Cao, X., Peyron, O., Nazarova, L.,
964 Novenko, E.Y., Park, J. Regional pollen-based Holocene temperature and precipitation patterns depart from
965 the Northern Hemisphere mean trends. *Clim. Past*, 19(7), 1481-1506, 2023.
- 966 Hes, G., Sanchez-Goñi, M.F., and Bouttes, N. Impact of terrestrial biosphere on the atmospheric
967 CO₂ concentration across Termination V. *Clim. Past*, 18(6), 1429-1451, 2022. <https://doi.org/10.5194/cp-18-1429-2022>
- 968
- 969 Heusser, L. E. and Balsam, W. L. Pollen distribution in the north-east Pacific Ocean. *Quat. Res.* 7, 45-62, 1977.
- 970 Hodell, D. A., Channeil, J. E. T., Curtis, J. H., Romero, O. E., and Röhl, U. Onset of “Hudson Strait” Heinrich
971 events in the eastern North Atlantic at the end of the middle Pleistocene transition (~640 ka)?
972 *Paleoceanography* 23(4), 1-16, 2008. <https://doi.org/10.1029/2008PA001591>
- 973 Huntley, B. Europe. *Vegetation history* (ed. by B. Huntley and T. Webb III), pp. 341-383. Kluwer Academic
974 Publishers, Dordrecht, 1988.
- 975 IPCC. *Climate Change: Impacts, Adaptation and Vulnerability*. Accessible at:
976 <https://www.ipcc.ch/report/ar6/wg2/>, 2022.
- 977 Jalut, G., Dedouat, J. J., Fontugne, M., and Otto, T. Holocene circum-Mediterranean vegetation changes: Climate
978 forcing and human impact. *Quatern. Int.* 200, 4-18, 2009.
- 979 Joannin, S., Brugiapaglia, E., De Beaulieu, J.L., Bernardo, L., Magny, M., Peyron, O., Goring, S., and Vannièrè,
980 B. Pollen-based reconstruction of Holocene vegetation and climate in southern Italy: the case of Lago
981 Trifoglietti. *Clim. Past* 8(6), 1973-1996, 2012.
- 982 Jouzel, J., Masson-Delmotte, V., Cattani, O., Dreyfus, G., Falourd, S., Hoffmann, G., Minster, B., Nouet, J.,
983 Barnola, J.M., Chappellaz, J., Fischer, H., Gallet, J.C., Johnsen, S., Leuenberger, M., Loulergue, L., Luethi,
984 D., Oerter, H., Parrenin, F., Raisbeck, G., Raynaud, D., Schilt, A., Schwander, J., Selmo, E., Souchez, R.,
985 Spahni, R., Stauffer, B., Steffensen, J.P., Stenni, B., Stocker, T.F., Tison, J.L., Werner, M., Wolff, E.W. Orbital
986 and millennial Antarctic climate variability over the past 800,000 years. *Science* 317(5839), 793-796, 2007.
- 987 Juggins, S. Package “rioja” – Analysis of Quaternary Science Data. *The Comprehensive R Archive Network*, 2020.
- 988 Kaenel, E., Siesser, W.G., Murat, A. Pleistocene calcareous nannofossil biostratigraphy and the western
989 Mediterranean sapropels, Sites 974 to 977 and 979. In: Zhan, R., Comas, M.C., Klaus, A. (Eds.), *Proc. ODP*
990 *Sci. Results*. 161. College Station, Texas, 15-183, 1999.
- 991 Kallel, N., Paterne, M., Labeyrie, L., Duplessy, J.-C., and Arnold, M. Temperature and salinity records of the
992 Tyrrhenian Sea during the last 18,000 years. *Palaeogeogr. Palaeoclimatol. Palaeoecol.* 135, 97-108, 1997.
- 993 Kandiano, E.S., Bauch, H.A., Fahl, K., Helmke, J.P., Röhl, U., Pérez-Folgado, M., and Cacho, I. The meridional
994 temperature gradient in the eastern North Atlantic during MIS 11 and its link to the ocean-atmosphere system.
995 *Palaeogeogr. Palaeoclimatol. Palaeoecol.* 333, 24-39, 2012.
- 996 Kelly, M.R. The Middle Pleistocene of North Birmingham. *Philos. Trans. R. Soc. Lond.* B247, 533-592, 1964.
- 997 Kotthoff, U., Pross, J., Müller, U.C., Peyron, O., Schmiel, G., Schulz, H., and Bordon, A. Climate dynamics in
998 the borderlands of the Aegean Sea during formation of sapropel S1 deduced from a marine pollen record.
999 *Quat. Sci. Rev.* 27, 832-845, 2008. <https://doi.org/10.1016/j.quascirev.2007.12.001>
- 1000 Kousis, I., Koutsodendris, A., Peyron, O., Leicher, N., Francke, A., Wagner, B., Giaccio, B., Knipping, M., and
1001 Pross, J. Centennial-scale vegetation dynamics and climate variability in SE Europe during Marine Isotope
1002 Stage 11 based on a pollen record from Lake Ohrid. *Quat. Sci. Rev.* 190, 20-38, 2018.
1003 <https://doi.org/10.1016/j.quascirev.2018.04.014>
- 1004 Koutsodendris, A., Brauer, A., Pälike, H., Müller, U.C., Dulski, P., Lotter, A.F., and Pross, J. Sub-decadal to
1005 decadal-scale climate cyclicity during the Holsteinian interglacial (MIS 11) evidenced in annually laminated
1006 sediments. *Clim. Past* 7, 987-999, 2011.
- 1007 Koutsodendris, A., Pross, J., Müller, U. C., Brauer, A., Fletcher, W. J., Kühl, N., Kirilova, E., Verhagen, F. T. M.,
1008 Lücke, A., and Lotter, A. F. A short-term climate oscillation during the Holsteinian interglacial (MIS 11c): An
1009 analogy to the 8.2ka climatic event? *Glob. Planet. Change* 92-93, 224-235, 2012.
1010 <https://doi.org/10.1016/j.gloplacha.2012.05.011>
- 1011 Koutsodendris, A., Kousis, I., Peyron, O., Wagner, B., and Pross, J. The Marine Isotope Stage 12 pollen record
1012 from Lake Ohrid (SE Europe): Investigating short-term climate change under extreme glacial conditions. *Quat.*
1013 *Sci. Rev.* 221, 105873, 2019.
- 1014 Koutsodendris, A., Dakos, V., Fletcher, W.J., Knipping, M., Kotthoff, U., Milner, A.M., Müller, U.C., Kaboth-
1015 Bahr, S., Kern, O.A., Kolb, L., and Vakhrameeva, P. Atmospheric CO₂ forcing on Mediterranean biomes
1016 during the past 500 kyrs. *Nat. Commun.* 14(1), 1664, 2023.
- 1017 Kukla, G. Continental records of MIS 11. *Washington DC American Geophysical Union Geophysical Monograph*
1018 *Series* 137, 207-211, 2003.
- 1019 Kukla, G., McManus, J. F., Rousseau, D.-D., and Chuine, I. How long and how stable was the last interglacial?
1020 *Quat. Sci. Rev.* 16, 605-612, 1997.



- 1021 Leroy, S.A.G., Henry, P., Peyron, O., Rostek, F., Kende, J., Bard, E., and Tachikawa, K. Palynology,
1022 palaeoclimate and chronology from the Saalian Glacial to Saint-Germain II interstadial from two long cores
1023 at the limit between the Mediterranean and Euxinian regions. *Quat. Sci. Rev.* 311, 108145, 2023.
- 1024 Lionello, P., Scarascia, L. The relation between climate change in the Mediterranean region and global warming.
1025 *Reg. Environ. Chang.* 18, 1481–1493, 2018.
- 1026 Liu, M., Shen, Y., González-Sampériz, P., Gil-Romera, G., Ter Braak, C.J., Prentice, I.C. and Harrison, S.P.
1027 Holocene climates of the Iberian Peninsula: pollen-based reconstructions of changes in the west-east gradient
1028 of temperature and moisture. *Clim. Past* 19, 803–834, 2023. <https://doi.org/10.5194/cp-19-803-2023>
- 1029 Loulergue, L., Schilt, A., Spahni, R., Masson-Delmotte, V., Blunier, T., Lemieux, B., Barnola, J.M., Raynaud,
1030 D., Stocker, T.F., Chappellaz, J. Orbital and millennial-scale features of atmospheric CH₄ over the past
1031 800,000 years. *Nature* 453, 383–386, 2008.
- 1032 Loutre, M.F., Berger, A. Marine Isotope Stage 11 as an analogue for the present interglacial. *Glob. Planet. Change*
1033 36, 209–217, 2003. [https://doi.org/10.1016/S0921-8181\(02\)00186-8](https://doi.org/10.1016/S0921-8181(02)00186-8)
- 1034 Ludwig, P., Shao, Y., Kehl, M. and Weniger, G.C. The Last Glacial Maximum and Heinrich event I on the Iberian
1035 Peninsula: A regional climate modelling study for understanding human settlement patterns. *Glob. Planet.*
1036 *Change* 170, 34–47, 2018.
- 1037 Magny, M., Miramont, C. and Sivan, O. Assessment of the impact of climate and anthropogenic factors on
1038 Holocene Mediterranean vegetation in Europe on the basis of palaeohydrological records. *Palaeogeogr.*
1039 *Palaeoclimatol. Palaeoecol.* 186(1-2), 47–59, 2002.
- 1040 Maiorano, P., Bertini, A., Capolongo, D., Eramo, G., Gallicchio, S., Girona, A., Pinto, D., Toti, F., Ventrucci, G.,
1041 Marino, M. Climate signatures through the marine isotope stage 19 in the Montalbano Jonico section (southern
1042 Italy): a land-sea perspective. *Palaeogeogr. Palaeoclimatol. Palaeoecol.* 461, 341–361, 2016.
- 1043 Marino, M., Girona, A., Maiorano, P., Di Renzo, R., Piscitelli, A., and Flores, J. A. Calcareous plankton and the
1044 mid-Brunhes climate variability in the Alboran Sea (ODP Site 977). *Palaeogeogr. Palaeoclimatol.*
1045 *Palaeoecol.* 508, 91–106, 2018. <https://doi.org/10.1016/j.palaeo.2018.07.023>
- 1046 Marriner, N., Kaniewski, D., Pourkerman, M. and Devillers, B. Anthropocene tipping point reverses long-term
1047 Holocene cooling of the Mediterranean Sea: A meta-analysis of the basin's Sea Surface Temperature records.
1048 *Earth-Sci Rev* 227, 103986, 2022.
- 1049 Martrat, B., Grimalt, J.O., Lopez-Martinez, C., Cacho, I., Sierro, F.J., Flores, J.A., Zahn, R., Canals, M., Curtis,
1050 J.H. and Hodell, D.A. Abrupt temperature changes in the Western Mediterranean over the past 250,000 years.
1051 *Science* 306(5702), 1762–1765, 2004.
- 1052 Martin, C., Menot, G., Thouveny, N., Peyron, O., Andrieu-Ponel, V., Montade, V., Davtian, N., Reille, M. and
1053 Bard, E. Early Holocene thermal maximum recorded by branched tetraethers and pollen in Western Europe
1054 (Massif Central, France). *Quat. Sci. Rev.* 228, 106109, 2020.
- 1055 Martrat, B., Jimenez-Amat, P., Zahn, R. and Grimalt, J.O. Similarities and dissimilarities between the last two
1056 deglaciations and interglaciations in the North Atlantic region. *Quat. Sci. Rev.* 99, 122–134, 2014.
- 1057 Masson-Delmotte, V., Landais, A., Combourieu-Nebout, N., von Grafenstein, U., Jouzel, J., Caillon, N.,
1058 Chappellaz, J., Dahl-Jensen, D., Johnsen, S.J. and Stenni, B. Variabilité climatique rapide pendant les périodes
1059 chaudes et froides aux pôles et en Europe. *Comptes rendus. Géoscience* 337(10-11), 935–946, 2005.
- 1060 Mauri, A., Davis, B., Collins, P. M., and Kaplan, J. The climate of Europe during the Holocene: A gridded pollen-
1061 based reconstruction and its multi-proxy evaluation. *Quat. Sci. Rev.* 112, 109–127, 2015.
- 1062 Mayewski, P.A., Rohling, E.E., Stager, J.C., Karlen, W., Maasch, K.A., Meeker, L.D., Meyerson, E.A., Gasse,
1063 F., van Kreveld, S., Holmgren, K., Lee-Thorp, J., Rosqvist, G., Rack, F., Staubwasser, M., Schneider, R.R.,
1064 Steig, E.J. Holocene climate variability. *Quat. Res.* 62, 243–255, 2004.
- 1065 McManus, J.F., Oppo, D.W., Cullen, J.L. and Healey, S. Marine isotope stage 11 (MIS 11): analog for Holocene
1066 and future climate? *Washington DC American Geophysical Union Geophysical Monograph Series* 137, 69–
1067 85, 2003.
- 1068 MedECC. Climate and Environmental Change in the Mediterranean Basin – Current Situation and Risks for the
1069 Future. In: *Climate and Environmental Change in the Mediterranean Basin – Current Situation and Risks for*
1070 *the Future. First Mediterranean Assessment Report*, edited by W. Cramer, J. Guiot and K. Marini, 60.
1071 Marseille: Union for the Mediterranean, 2020.
- 1072 Moncel, M. H., Arzarello, M., and Peretto, C. The Holsiteinian period in Europe (MIS 11-9). *Quat. Int.* 409, 1–8,
1073 2016.
- 1074 Moreno, A., Cacho, I., Canals, M., Grimalt, J.O., Sanchez Vidal, A. Millennial-scale variability in the productivity
1075 signal from the Alboran Sea record, western Mediterranean Sea. *Palaeogeogr. Palaeoclimatol. Palaeoecol.*
1076 211(3-4), 205–219, 2004.
- 1077 Naughton, F., Sánchez Gofí, M. F., Desprat, S., Turon, J. L., Duprat, J., Malaizé, B., Joli, C., Cortijo, E., Drago,
1078 T., and Freitas, M. C. Present-day and past (last 25,000 years) marine pollen signal off western Iberia. *Mar.*
1079 *Micropaleontol.* 62, 91–114, 2007.



- 1080 Nehrbaas-Ahles, C., Shin, J., Schmitt, J., Bereiter, B., Joos, F., Schilt, A., Schmidely, L., Silva, L., Teste, G.,
1081 Grilli, R. and Chappellaz, J. Abrupt CO₂ release to the atmosphere under glacial and early interglacial climate
1082 conditions. *Science* 369(6506), 1000-1005, 2020.
- 1083 Nomade, S., Bassinot, F., Marino, M., Simon, Q., Dewilde, F., Maiorano, P., Isguder, G., Blamart, D., Girone,
1084 A., Scao, V., Pereira, A., Toti, F., Bertini, A., Combourieu-Nebout, N., Peral, M., Bourles, D.L., Petrosino, P.,
1085 Gallicchio, S., Ciaranfi, N. High-resolution foraminifer stable isotope record of MIS 19 at Montalbano Jonico,
1086 southern Italy: a window into Mediterranean climatic variability during a low-eccentricity interglacial. *Quat.*
1087 *Sci. Rev.* 205, 106-125, 2019.
- 1088 NorthGRIP Members. High-resolution record of Northern Hemisphere climate extending into the last interglacial
1089 period. *Nature*, 431: 147–151, 2004.
- 1090 Oliveira, D., Desprat, S., Rodrigues, T., Naughton, F., Hodell, D., Trigo, R., Rufino, M., Lopes, C., Abrantes, F.,
1091 and Sánchez Goñi, M. F. The complexity of millennial-scale variability in southwestern Europe during MIS
1092 11. *Quat. Res.* (United States), 86(3), pp.373–387. <https://doi.org/10.1016/j.yqres.2016.09.002>, 2016.
- 1093 Olson, S.L., Hearty, P.J.A. A sustained 121m sea level highstand during MIS 11 (400 ka): direct fossil and
1094 sedimentary evidence from Bermuda. *Quat Sci Rev* 28, 271–285, 2009.
- 1095 Ortíz, Trinidad. Torres, Antonio Delgado, J.F. Llamas, Vicente Soler, Maruja Valle, Ramón Julià, Laura Moreno,
1096 Arantxa Díaz-Bautista. Palaeoenvironmental changes in the Padul Basin (Granada, Spain) over the last 1Ma
1097 based on the biomarker content, *Palaeogeogr. Palaeoclimatol. Palaeoecol.*, 298, 286-299, ISSN 0031-0182,
1098 2010. <https://doi.org/10.1016/j.palaeo.2010.10.003>.
- 1099 Ozenda, P. Sur les étages de végétation dans les montagnes du bassin méditerranéen. *Documents de Cartographie*
1100 *Ecologique*, 16, pp.1–32, 1975.
- 1101 Past Interglacials Working Group of PAGES. Interglacials of the last 800,000 years. *Reviews of Geophysics*, 54(1),
1102 162-219, 2016.
- 1103 Peñalba, M.C., Maurice, A., Guiot, J., Duplessy, J.C., de Beaulieu, J.L. Termination of the last glaciation in the
1104 Iberian Peninsula Inferred from the Pollen Sequence of Quintanar de la Sierra. *Quat. Res.* 48, 205–214, 1997.
- 1105 Pérez-Folgado, M., Sierro, F.J., Flores, J.A., Grimalt, J.O. and Zahn, R. Paleoclimatic variations in foraminifer
1106 assemblages from the Alboran Sea (Western Mediterranean) during the last 150 ka in ODP Site 977. *Mar.*
1107 *Geol.*, 212(1-4),113-131, 2004.
- 1108 Peyron, O., Combourieu-Nebout, N., Brayshaw, D., Goring, S., Andrieu-Ponel, V., Desprat, S., Fletcher, W.,
1109 Gambin, B., Ioakim, C., Joannin, S., Kotthoff, U., Kouli, K., Montade, V., Pross, J., Sadori, L., Magny, M.
1110 Precipitation changes in the Mediterranean basin during the Holocene from terrestrial and marine pollen
1111 records: a model-data comparison. *Clim. Past*, 13, 249-265, <https://doi.org/10.5194/cp-13-249-2017>, 2017.
- 1112 Peyron, O., Goring, S., Dormoy, I., Kotthoff, U., Pross, J., De Beaulieu, J.L., Drescher-Schneider, R., Vanniere,
1113 B., Magny, M. Holocene seasonality changes in the central Mediterranean region reconstructed from the pollen
1114 sequences of Lake Accesa (Italy) and Tenaghi Philippon (Greece). *Holocene* 21, 131-146,
1115 <https://doi.org/10.1177/0959683610384162>, 2011.
- 1116 Peyron, O., Magny, M., Goring, S., Joannin, S., De Beaulieu, J.L., Brugiapaglia, E., Sadori, L., Garfi, G., Kouli,
1117 K., Ioakim, C. and Combourieu-Nebout, N. Contrasting patterns of climatic changes during the Holocene
1118 across the Italian Peninsula reconstructed from pollen data. *Clim. Past*, 9(3), pp.1233-1252, 2013.
- 1119 Pol, K., Masson Delmotte, V., Johnsen, S., Bigler, M., Cattani, O., Durand, G., Falourd, S., Jouzel, J., Minster,
1120 B., Parrenin, F., Ritz, C., Steen Larsen C. H., Stenni, B. New MIS 19 EPICA Dome C high resolution
1121 deuterium data: hints for a problematic preservation of climate variability at sub-millennial scale in the “oldest
1122 ice”. *Earth Planet Sci. Lett.* 298, 95-103, 2010.
- 1123 Pons, A. and Reille, M. The Holocene and Upper Pleistocene pollen record from Padul (Granada, Spain): a new
1124 study, *Palaeogeogr. Palaeoclimatol. Palaeoecol.*, 66, 243–263, 1988.
- 1125 Pross, J., Christianis, K., Fischer, T., Fletcher, W.J., Hardiman, M., Kalaitzidis, S., Knipping, M., Kotthoff, U.,
1126 Milner, A.M., Muller, U.C. and Schmiiedl, G. The 1.35-Ma-long terrestrial climate archive of Tenaghi
1127 Philippon, northeastern Greece: Evolution, exploration, and perspectives for future research. *Newsletters on*
1128 *Stratigraphy*, 48(3), 253-276, 2015.
- 1129 Pross, J., Kotthoff, U., Müller, U. C., Peyron, O., Dormoy, I., Schmiiedl, G., Kalaitzidis, S., and Smith, A. M.
1130 Massive perturbation in terrestrial ecosystems of the Eastern Mediterranean region associated with the 8.2 kyr
1131 B.P. climatic event, *Geology*, 37, 887–890, 2009.
- 1132 Quézel, P. and Médail, F. *Ecologie et biogéographie des forêts du bassin méditerranéen*, Elsevier-Lavoisier eds,
1133 Paris, France, 571 pp., 2003.
- 1134 Ramos-Román, M.J., Jiménez-Moreno, G., Camuera, J., García-Alix, A., Anderson, R.S., Jiménez-Espejo, F.J.
1135 and Carrión, J.S. Holocene climate aridification trend and human impact interrupted by millennial-and
1136 centennial-scale climate fluctuations from a new sedimentary record from Padul (Sierra Nevada, southern
1137 Iberian Peninsula). *Clim. Past*, 14(1),117-137, 2018.
- 1138 Raymo, M.E. and Mitrovica, J.X. Collapse of polar ice sheets during the stage 11 interglacial. *Nature*, 483(7390),
1139 453-456, 2012.



- 1140 Regattieri, E., Giaccio, B., Galli, P., Nomade, S., Peronace, E., Messina, P., Sposato, A., Boschi, C., Gemelli, M.
1141 A multi-proxy record of MIS 11-12 deglaciation and glacial MIS 12 instability from the Sulmona Basin
1142 (central Italy). *Quat Sci Rev* 132, 12-145, 2016.
- 1143 Reille, M., and de Beaulieu, J. L. Long Pleistocene pollen records from the Praclaux crater, south-central France.
1144 *Quat. Res.*, 44(2), 205–215. <https://doi.org/10.1006/qres.1995.1065>, 1995.
- 1145 Rivas-Martínez, S. Bioclimatic stages, chorological sectors and series of vegetation in Mediterranean Spain. *Ecol.*
1146 *mediterr.*, 8(1), 275-288, 1982.
- 1147 Robles M., Peyron O., Ménot G., Brugiapaglia E., Wulf S., Appelt O., Blache M., Vannièrè B., Dugerdil L., Paura
1148 B., Ansanay-Alex S., Cromartie A., Charlet L., Guédron S., de Beaulieu JL, and Joannin, S. Climate changes
1149 during the Lateglacial in South Europe: new insights based on pollen and brGDGTs of Lake Matese in Italy,
1150 *Clim. Past*, 19, 493–515, <https://doi.org/10.5194/cp-19-493-2023>, 2023.
- 1151 Rodrigo-Gámiz, M., García-Alix, A., Jiménez-Moreno, G., Ramos-Román, M.J., Camuera, J., Toney, J.L.,
1152 Sachse, D., Anderson, R.S. and Damsté, J.S.S. Paleoclimate reconstruction of the last 36 kyr based on
1153 branched glycerol dialkyl glycerol tetraethers in the Padul palaeolake record (Sierra Nevada, southern Iberian
1154 Peninsula). *Quat Sci Rev*, 281, p.107434, 2022.
- 1155 Rodrigues, T., Voelker, A.H.L., Grimalt, J.O., Abrantes, F., Naughton, F. Iberian Margin sea surface temperature
1156 during MIS 15 to 9 (580-300 ka): glacial sub-orbital variability versus interglacial stability. *Paleoceanography*
1157 26, 1e16, <https://doi.org/10.1029/2010PA001927>, 2011.
- 1158 Rohling, E.J., Fenton, M., Jorissen, F.J., Bertrand, P., Ganssen, G., Caulet, J.P. Magnitudes of sea-level lowstands
1159 of the past 500,000 years. *Nature* 394, 162e165, <https://doi.org/10.1038/28134>, 1998.
- 1160 Rossignol-Strick, M. The Holocene climatic optimum and pollen records of sapropel 1 in the Eastern
1161 Mediterranean, 9000–6000 BP. *Quat. Sci. Rev.* 18, 515–530, 1999.
- 1162 Ruddiman, W.F. The anthropogenic greenhouse era began thousands of years ago. *Climatic change*, 61(3), 261-
1163 293, 2003.
- 1164 Ruddiman, W.F. The early anthropogenic hypothesis: Challenges and responses. *Rev Geophys*, 45(4), 2007.
- 1165 Ruddiman, W.F., Fuller, D.Q., Kutzbach, J.E., Tzedakis, P.C., Kaplan, J.O., Ellis, E.C., Vavrus, S.J., Roberts,
1166 C.N., Fyfe, R., He, F. and Lemmen, C. Late Holocene climate: Natural or anthropogenic? *Rev Geophys*, 54(1),
1167 93-118, 2016.
- 1168 Sadori, L., Ortu, E., Peyron, O., Zanchetta, G., Vannièrè, B., Desmet, M. and Magny, M. The last 7 millennia of
1169 vegetation and climate changes at Lago di Pergusa (central Sicily, Italy). *Clim. Past*, 9(4), pp.1969-1984, 2013.
- 1170 Sadori, L., Koutsodendris, A., Panagiotopoulos, K., Masi, A., Bertini, A., Combourieu-Nebout, N., Francke, A.,
1171 Kouli, K., Joannin, S., Mercuri, A.M. and Peyron, O. Pollen-based paleoenvironmental and paleoclimatic
1172 change at Lake Ohrid (south-eastern Europe) during the past 500 ka. *Biogeosciences*, 13(5), pp.1423-1437,
1173 2016.
- 1174 Salonen, J.S., Korpela, M., Williams, J.W., Luoto, M. Machine-learning based reconstructions of primary and
1175 secondary climate variables from North American and European fossil pollen data. *Sci. Rep.* 9, 1–13,
1176 <https://doi.org/10.1038/s41598-019-52293-4>, 2019.
- 1177 Salonen, J.S., Luoto, M., Alenius, T., Heikkilä, M., Seppä, H., Telford, R.J. and Birks, H.J.B. Reconstructing
1178 palaeoclimatic variables from fossil pollen using boosted regression trees: comparison and synthesis with other
1179 quantitative reconstruction methods. *Quat Sci Rev*, 88, 69-81, 2014.
- 1180 Sánchez Goñi, M. F., Llave, E., Oliveira, D., Naughton, F., Desprat, S., Ducassou, E., Hodell, D. A., and
1181 Hernández-Molina, F. J. Climate changes in southwestern Iberia and Mediterranean Outflow variations during
1182 two contrasting cycles of the last 1 Myrs: MIS 31-MIS 30 and MIS 12-MIS 11. *Glob. Planet. Change*, 136,
1183 18–29, <https://doi.org/10.1016/j.gloplacha.2015.11.006>, 2016.
- 1184 Sánchez Goñi, M., Eynaud, F., Turon, J. L., and Shackleton, N. J. High resolution palynological record off the
1185 Iberian margin: direct land-sea correlation for the Last Interglacial complex. *Earth Planet Sci Lett*, 171(1),
1186 123-137, 1999.
- 1187 Sánchez Goñi, M.F., Bakker, P., Desprat, S., Carlson, A.E., Van Meerbeek, C.J., Peyron, O., Naughton, F.,
1188 Fletcher, W.J., Eynaud, F., Rossignol, L. and Renssen, H. European climate optimum and enhanced Greenland
1189 melt during the Last Interglacial. *Geology*, 40(7), pp.627-630, 2012.
- 1190 Sassoon, D., Lebreton, V., Combourieu-Nebout, N., Peyron, O. and Moncel, M.H. Palaeoenvironmental Changes
1191 in the Southwest Mediterranean (ODP Site 976, Alboran Sea) During the MIS 12/11 Transition and the MIS
1192 11 Interglacial. *Quat Sci Rev*, 304: 108010.
- 1193 Shackleton, N.J., Sánchez-Goñi, M.F., Pailler, D. and Lancelot, Y. Marine isotope substage 5e and the Eemian
1194 interglacial. *Glob. Planet. Change*, 36(3), 151-155, 2003.
- 1195 Shipboard Scientific Party. Site 976. In: *Comas, M.C., Zahn, R., Klaus, A., et al. (Eds.), Proc. ODP, Init. Repts.*,
1196 *vol. 161. Ocean Drilling Program*, College Station, TX, pp. 179-297, 1996.
- 1197 Siani, G., Michel, E., De Pol-Holz, R., DeVries, T., Lamy, F., Carel, M., Isguder, G., Dewilde, F. and Laurantou,
1198 A. Carbon isotope records reveal precise timing of enhanced Southern Ocean upwelling during the last
1199 deglaciation. *Nat. Commun.*, 4(1), p.2758, 2013.



- 1200 Sinopoli, G., Peyron, O., Masi, A., Holtvoeth, J., Francke, A., Wagner, B. and Sadori, L. Pollen-based temperature
1201 and precipitation changes in the Ohrid Basin (western Balkans) between 160 and 70 ka. *Clim. Past*, 15(1), 53-
1202 71, 2019.
- 1203 ter Braak, C.J.F., Juggins, S. Weighted averaging partial least squares regression (WA-PLS): an improved method
1204 for reconstructing environmental variables from species assemblages. *Hydrobiologia* 269–270, 485–502,
1205 <https://doi.org/10.1007/BF00028046>, 1993.
- 1206 Toti, F., Bertini, A., Gironi, A., Marino, M., Maiorano, P., Bassinot, F., Combourieu-Nebout, N., Nomade, S.,
1207 and Buccianti, A. Marine and terrestrial climate variability in the western Mediterranean Sea during marine
1208 isotope stages 20 and 19. *Quat Sci Rev*, 243, <https://doi.org/10.1016/j.quascirev.2020.106486>, 2020.
- 1209 Turner, C. The Middle Pleistocene deposits at Marks Tey, Essex. *Philosophical Transactions of the Royal Society
1210 of London, Series B* 257, 373–440, 1970.
- 1211 Turon, J.-L., Lézine, A.-M., and Denèfle, M. Land–sea correlations for the last deglaciation inferred from a pollen
1212 and dinocyst record from the Portuguese margin, *Quat. Res.*, 59, 88–96, 2003.
- 1213 Tye, G.J., Sherriff, J., Candy, I., Coxon, P., Palmer, A., Mcclymont, E.L., Schreve, D.C. The $\delta 18\text{O}$ stratigraphy
1214 of the Hoxnian lacustrine sequence at Marks Tey, Essex, UK: implications for the climatic structure of MIS
1215 11 in Britain. *J. Quat. Sci.* 31, 75–92, <https://doi.org/10.1002/jqs.2840>, 2016.
- 1216 Tzedakis, P. C., Hodell, D. A., Nehrbass-Ahles, C., Mitsui, T., and Wolff, E. W. Marine Isotope Stage 11c: An
1217 unusual interglacial. *Quat Sci Rev*, 284, 107493, <https://doi.org/10.1016/j.quascirev.2022.107493>, 2022.
- 1218 Tzedakis, P. C., Hooghiemstra, H., and Pälike, H. The last 1.35 million years at Tenaghi Philippon: revised
1219 chronostratigraphy and long-term vegetation trends. *Quat Sci Rev*, 25(23–24), 3416–3430,
1220 <https://doi.org/10.1016/j.quascirev.2006.09.002>, 2006.
- 1221 Tzedakis, P.C. The MIS 11–MIS 1 analogy, southern European vegetation, atmospheric methane and the "early
1222 anthropogenic hypothesis". *Clim. Past*, 6(2), 131–144, 2010.
- 1223 Tzedakis, P.C., Channell, J.E.T., Hodell, D.A., Kleiven, H.F. and Skinner, L.C. Determining the natural length of
1224 the current interglacial. *Nat Geosci*, 5(2), 138–141, 2012.
- 1225 Vavrus, S.J., He, F., Kutzbach, J.E. et al. Glacial Inception in Marine Isotope Stage 19: An Orbital Analog for a
1226 Natural Holocene Climate. *Sci. Rep.*, 8, 10213, <https://doi.org/10.1038/s41598-018-28419-5>, 2018.
- 1227 Vázquez Riveiros, N., Waelbroeck, C., Skinner, L., Duplessy, J. C., McManus, J. F., Kandiano, E. S., and Bauch,
1228 H. A. The “MIS 11 paradox” and ocean circulation: Role of millennial scale events. *Earth Planet Sci Lett*,
1229 371–372, 258–268, <https://doi.org/10.1016/j.epsl.2013.03.036>, 2013.
- 1230 Voelker, A. H. L., Rodrigues, T., Billups, K., Oppo, D., McManus, J., Stein, R., Hefter, J., and Grimalt, J. O.
1231 Variations in mid-latitude North Atlantic surface water properties during the mid-Brunhes (MIS 9–14) and
1232 their implications for the thermohaline circulation. *Clim. Past*, 6(4), 531–552, <https://doi.org/10.5194/cp-6-531-2010>, 2010.
- 1234 Wang, Y., Yang, X., Wang, Y., Wang, Q., and Edwards, R. L. The structure of marine isotope Stage 11 and its
1235 alignment with the Holocene. *Palaeogeogr. Palaeoclimatol. Palaeoecol.*, 609, 111311,
1236 <https://doi.org/10.1016/j.palaeo.2022.111311>, 2023.
- 1237 Watts, W. A., Allen, J. R. M., Huntley, B., and Fritz, S. C. Vegetation history and climate of the last 15 000 years
1238 at Laghi di Monticchio, Southern Italy, *Quaternary Sci. Rev.*, 15, 113–132, 1996.
- 1239 West, R. The Quaternary deposits at Hoxne, Suffolk. *Philosophical Transactions of the Royal Society London.
1240 Series B* 239, 265–356, 1956.
- 1241 Wijmstra, T. A. and Smit, A. Palynology of the middle part (30–78 metres) of the 120 m deep section in Northern
1242 Greece (Macedonia). *Acta Bot. Neerl.* 25, 297–312, 1976.
- 1243 Yin, Q., and Berger, A. Interglacial analogues of the Holocene and its natural near future. *Quat Sci Rev*, 120, 28–
1244 46, <https://doi.org/10.1016/j.quascirev.2015.04.008>, 2015.
- 1245 Zhuravleva, A. *Paleoceanographic and climatic teleconnections between the subarctic and subtropical North
1246 Atlantic during the last interglacial (MIS 5e)*. Doctoral dissertation.
1247 <https://doi.org/10.13140/RG.2.2.26501.86242>, 2018.
- 1248 Zonneveld, K.A. Palaeoclimatic reconstruction of the last deglaciation (18–8 ka BP) in the Adriatic Sea region; a
1249 land-sea correlation based on palynological evidence. *Palaeogeogr. Palaeoclimatol. Palaeoecol.*, 122(1–4),
1250 89–106.